J|A|C|S ARTICLES

Published on Web 03/16/2010

DFT-NMR Investigation and ^{51}V 3QMAS Experiments for Probing Surface OH Ligands and the Hydrogen-Bond Network in a Polyoxovanadate Cluster: The Case of $Cs_4[H_2V_{10}O_{28}]\cdot 4H_2O$

Lionel A. Truflandier,*[,†,‡] Florent Boucher,[†] Christophe Payen,[†] Redouane Hajjar,[§] Yannick Millot,[§] Christian Bonhomme,[||] and Nathalie Steunou[||]

Institut des Matériaux Jean Rouxel (IMN), Université de Nantes, UMR CNRS 6502, 2 rue de la Houssinière, BP 32229, 44340 Nantes Cedex 3, France, Laboratoire des Systèmes Interfaciaux à l'Echelle Nanométrique (SIEN), UMR CNRS 7142, UPMC Univ Paris 06, 4 place Jussieu, 75252 Paris Cedex 05, France, and Laboratoire de Chimie de la Matière Condensée de Paris (LCMCP), UMR CNRS 7574, UPMC Univ Paris 06, Collège de France, 11 place Marcelin Berthelot, 75231 Paris Cedex 05, France

Received October 21, 2009; E-mail: lionel.truflandier@gmail.com

Abstract: This work shows that the combination of first-principles calculations and ^{51}V NMR experiments is a powerful tool to elucidate the location of surface hydroxyl groups and to precisely describe the hydrogen bond network in the complex decavanadate cluster $Cs_4[H_2V_{10}O_{28}].4H_2O$, enhancing the strength of NMR crystallography. The detailed characterization of H-bond networks for these kinds of inorganic compounds is of primary importance and should benefit from the DFT-NMR predictions by considering explicitly the periodic boundary conditions. The determination of the $Cs_4[H_2V_{10}O_{28}]\cdot 4H_2O$ structure by single-crystal X-ray diffraction was not sufficiently accurate to provide the location of protons. From available diffraction data, five different protonated model structures have been built and optimized using DFT-based methods. The possible interconversion of two decavanadate isomers through a proton exchange is evaluated by calculating the energy barrier and recording variable-temperature ^{1}H MAS NMR spectra. First-principles calculations of ^{51}V NMR parameters clearly indicate that these parameters are very sensitive to the local intermolecular hydrogen-bonding interactions. Considering the DFT error limits, the fairly good agreement between calculated and experimental NMR parameters arising from the statistical modeling of the data allows the unambiguous assignment of the five ^{51}V NMR signals and, thus, the location of OH surface ligands in the decavanadate cluster. In particular, first-principles calculations accurately reproduce the ^{51}V quadrupolar parameters. These results are fully consistent with ^{51}V 3QMAS NMR spectra recorded with and without ^{1}H decoupling. Finally, correlations are established between local octahedral VO_6 deformations and ^{51}V NMR parameters (C_q and $\Delta\delta$), which will be useful for the characterization of a wide range of chemical species containing vanadium(V).

1. Introduction

For several years, the combination of theory (including quantum mechanics (QM) and classical molecular mechanics (MM) methods), diffraction techniques (X-ray and/or neutron), and magnetic/electronic resonance experiments (nuclear magnetic resonance (NMR) and electronic paramagnetic resonance (EPR)) has offered great opportunities for the accurate resolution of complex structures. This approach can be considered as iterative in the following sense: starting from an initial model (derived for instance from X-ray diffraction data), spectroscopic data are then calculated from first-principles and compared to experimental magnetic resonance parameters. Such parameters then act as constraints on the initial model. Therefore, this initial model can be refined up to the point where experimental and calculated spectroscopic data converge. This methodology seems promising when protons are involved in the corresponding structure. In fact, the precise location of protons is rarely achieved by using standard X-ray crystallography methods. In this case, the refinement of geometry based on the combination of molecular and solid-state theories with NMR/EPR spectroscopy is of paramount importance and is a unique approach for accurate proton location.

For aperiodic models involved in computational biomolecular chemistry, the reliablility of combined QM/MM methods is now well established, enabling the detailed study of enzymatic reactivity as well as many other applications, such as the calculation of spectroscopic and excited-states properties which appear to be very promising for full interpretation of NMR/EPR data and refinement of initial structural hypotheses.[1] We give here two examples of studies reported recently in the literature and related to peroxidase and rhodopsin. Waller et al. studied in depth QM/MM models of

[†] IMN Université de Nantes.

[‡] Current address: Department of Chemistry, 312 Natural Sciences Complex, State University of New York at Buffalo, Buffalo, NY 14260-3000.

[§] Laboratoire des Systèmes Interfaciaux à l'Echelle Nanométrique, UPMC Université de Paris 06.

[||] Laboratoire de Chimie de la Matière Condensée de Paris, UPMC Université de Paris 06.

(1) Senn, H. M.; Thiel, W. *Angew. Chem., Int. Ed.* **2009**, *48*, 1198–1229.

vanadium chloroperoxidase in connection with ^{51}V NMR experimental data (isotropic chemical shift and anisotropic chemical shift (CSA) parameters).[2] Several models exhibiting various H-bond networks were optimized. Consequently, some of them were safely excluded on the basis of clear disagreement regarding the corresponding ^{51}V CSA calculated data. Pooransingh et al. combined ^{51}V MAS spectroscopy and DFT calculations in the case of the active site in vanadium haloperoxidase.[3] Recently, Gansmüller et al. emphasized the importance of accurate X-ray diffraction *and* NMR data as a safe starting point for improving QM/MM models in the framework of biological photochemical processes.[4] In the case of rhodopsin, Gascon et al. proved that QM/MM modeling and $^{1}H/^{13}C$ NMR were able to characterize bond conformation, isomerization, and chromophore environment.[5] The rhodopsin chromophore in the dark state of the protein, as well as the photointermediate bathorhodopsin, were also extensively studied by QM/MM/NMR by Röhrig et al.[6]

EPR-derived techniques are also powerful methods of investigation for the location of protons in proteins and complex solids. For instance, measurement of large distances—up to 80 Å—between spins can be performed by manipulating the dipolar couplings in PELDOR (pulsed electron electron double resonance) experiments.[7,8] HYSCORE (hyperfine sublevel correlation spectroscopy) experiments are also extremely useful for the description of protein structure by recovering weak anisotropic hyperfine interactions. For example, multifrequency HYSCORE experiments were performed by Garcia-Rubio et al. for the case of high-spin aquometmyoglobin, leading to the full EPR characterization of remote protons and to the distinction of two different protons in water ligands.[9] Dube et al. probed the existence of a hydrogen bond to coordinated O_2 in a myoglobin/hemoglobin system by pulsed-EPR spectroscopy.[10] Quinones were recently studied in the frame of solar energy transduction.[11] Hydrogen-bonding interactions are of prime importance and were successfully studied by a combination of continuous wave EPR and HYSCORE experiments. In another work,[12] exchangeable protons with different hyperfine couplings were evidenced near the semiquinone radical of the cytochrome bo3 from *E. coli*, demonstrating again the usefulness of HYSCORE experiments for the characterization of protons in proteins.

Currently, NMR crystallography,[13] which mainly refers to the significant use of solid-state NMR data for determining crystal structures, is a very useful tool in several areas of solid-state and materials sciences. Solid-state NMR data are often combined with diffraction data, but NMR methods are now sufficiently advanced that complete crystal structures have been determined without the need of diffraction experiments.[14,15] Furthermore, NMR can be coupled with first-principles calculations—mainly density functional theory (DFT)—for geometry optimization and/or NMR parameter predictions. Within this context, we can give recent examples of promising methodologies based on ^{29}Si double quantum and ^{1}H spin diffusion NMR, which have allowed the accurate resolution of crystal structures of zeolites and molecular crystals, respectively.[16−18] In the framework of biomolecules, it has been clearly demonstrated that ab initio calculations of NMR parameters enhance the protein structure refinement. Moreover, NMR anisotropies (such as CSA or dipolar interaction) can act as safe constraints for NMR refinement.[19] As an example, such an approach has been used by Oldfield and co-workers in the case of phenylalanine and tyrosine groups in dipeptides and proteins, and in the β_1-immunoglobulin binding domain of protein G.[20,21]

Conversely, a combination of experimental and theoretical NMR parameters can be used to probe the accuracy of X-ray diffraction (XRD) data,[22,23] allowing the validation or the correction of structure models.[24−28] In the latter case, DFT structure relaxation can be used as a refinement tool, bearing in mind the intrinsic inaccuracies of the ab initio method and the fact that the minimum-energy structure is ideally obtained at 0 K. In the field of solid-state chemistry, the growing application of NMR crystallography has been stimulated by the introduction of computationally tractable methods dedicated to the calculation of NMR parameters for extended periodic systems. Since condensed matter theory—applied to the electronic structure of solids—describes the electron interactions in a periodic potential, methods based on the combination of plane wave (PW) basis sets and pseudopotentials are better suited to study crystalline solids than are finite-cluster approaches. For these latter methods, it is well-known that, in order to accurately reproduce the long-range Coulomb part of the potential, the size of the cluster must be increased to a number of atoms that is computationally unaffordable. Consequently, the projector augmented-wave method (PAW)[29,30] and its gauge invariant extension (gauge-including projector augmented wave,[31] GIPAW) have been retained as the most promising methods for predicting the quadrupolar and chemical shift parameters in periodic systems. Nevertheless, whereas outstanding agreement is observed between experimental and GIPAW calculated chemical shift parameters of the elements belonging to the three first rows of the periodic table, a degradation of the method's reliability has been revealed for calcium and

(2) Waller, M. P.; Bühl, M.; Geethalakshmi, K.; Wang, D.; Thiel, W. *Chem. Eur. J.* **2007**, *13*, 4723–4732.
(3) Pooransingh, N.; Pomerantseva, E.; Ebel, M.; Jantzen, S.; Rehder, D.; Polenova, T. *Inorg. Chem.* **2003**, *42*, 1256–1266.
(4) Gansmüller, A.; Concistrè, M.; McLean, N.; Johannessen, O. G.; Marín-Montesinos, I.; Bovee-Geurts, P. H.; Verdegem, P.; Lugtenburg, J.; Brown, R. C.; DeGrip, W. J.; Levitt, M. H. *Biochim. Biophys. Acta* **2009**, *1788*, 1350–1357.
(5) Gascon, J. A.; Sproviero, E. M.; Batista, V. S. *J. Chem. Theory Comput.* **2005**, *1*, 674–685.
(6) Rohrig, U. F.; Sebastiani, D. *J. Phys. Chem. B* **2008**, *112*, 1267–1274.
(7) Prisner, T.; Rohrer, M.; MacMillan, F. *Annu. Rev. Phys. Chem.* **2001**, *52*, 279–313.
(8) Schiemann, O.; Prisner, T. F. *Q. Rev. Biophys.* **2007**, *40*, 1–53.
(9) García-Rubio, I.; Fittipaldi, M.; Trandafir, F.; Van Doorslaer, S. *Inorg. Chem.* **2008**, *47*, 11294–11304.
(10) Dube, H.; Kasumaj, B.; Calle, C.; Saito, M.; Jeschke, G.; Diederich, F. *Angew. Chem., Int. Ed.* **2008**, *47*, 2600–2603.
(11) Weyers, A. M.; Chatterjee, R.; Milikisiyants, S.; Lakshmi, K. V. *J. Phys. Chem. B* **2009**, *113*, 15409–15418.
(12) Yap, L. L.; Samoilova, R. I.; Gennis, R. B.; Dikanov, S. A. *J. Biol. Chem.* **2006**, *281*, 16879–16887.
(13) Harris, R. K.; Wasylishen, R. E.; Duer, M. J. *NMR Crystallography*; Wiley Blackwell: New York, 2009.
(14) Harris, R. K. *Solid State Sci.* **2004**, *6*, 1025–1037.
(15) Taulelle, F. *Solid State Sci.* **2004**, *6*, 1053–1057.
(16) Brouwer, D. H. *J. Am. Chem. Soc.* **2008**, *130*, 6306–6307.
(17) Pickard, C. J.; Salager, E.; Pintacuda, G.; Elena, B.; Emsley, L. *J. Am. Chem. Soc.* **2007**, *129*, 8932–8933.
(18) Salager, E.; Stein, R. S.; Pickard, C. J.; Elena, B.; Emsley, L. *Phys. Chem. Chem. Phys.* **2009**, *11*, 2610–2621.
(19) Grishaev, A.; Ying, J.; Bax, A. *J. Am. Chem. Soc.* **2006**, *128*, 10010–10011.
(20) Mukkamala, D.; Zhang, Y.; Oldfield, E. *J. Am. Chem. Soc.* **2007**, *129*, 7385–7392.
(21) Wylie, B. J.; Schwieters, C. D.; Oldfield, E.; Rienstra, C. M. *J. Am. Chem. Soc.* **2009**, *131*, 985–992.
(22) Harris, R. K.; Hodgkinson, P.; Pickard, C. J.; Yates, J. R.; Zorin, V. *Magn. Reson. Chem.* **2007**, *45*, S174–S186.
(23) Soleilhavoup, A.; Hampson, M. R.; Clark, S. J.; Evans, J. S. O.; Hodgkinson, P. *Magn. Reson. Chem.* **2007**, *45*, S144–S155.
(24) Ashbrook, S. E.; Polles, L. L.; Gautier, R.; Pickard, C. J.; Walton, R. I. *Phys. Chem. Chem. Phys.* **2006**, *8*, 3423–3431.
(25) Ashbrook, S. E.; Cutajar, M.; Pickard, C. J.; Walton, R. I.; Wimperis, S. *Phys. Chem. Chem. Phys.* **2008**, *10*, 5754–5764.
(26) Harris, R. K.; Joyce, S. A.; Pickard, C. J.; Cadars, S.; Emsley, L. *Phys. Chem. Chem. Phys.* **2006**, *8*, 137–143.
(27) Harris, R. K.; Cadars, S.; Emsley, L.; Yates, J. R.; Pickard, C. J.; Jetti, R. K. R.; Griesser, U. J. *Phys. Chem. Chem. Phys.* **2007**, *9*, 360–368.
(28) Yates, J. R.; Dobbins, S. E.; Pickard, C. J.; Mauri, F.; Ghi, P. Y.; Harris, R. K. *Phys. Chem. Chem. Phys.* **2005**, *7*, 1402–1407.
(29) Blöchl, P. E. *Phys. Rev. B* **1994**, *50*, 17953.
(30) Petrilli, H. M.; Blöchl, P. E.; Blaha, P.; Schwarz, K. *Phys. Rev. B* **1998**, *57*, 14690.
(31) Pickard, C. J.; Mauri, F. *Phys. Rev. B* **2001**, *63*, 245101.

vanadium oxide based compounds.[32−35] Indeed, such discrepancies are well-known to the quantum chemist community and have been discussed in the literature for many years, especially for the DFT calculation of 3d transition metal chemical shifts, such as those of ^{51}V.[36−42]

^{51}V, which is a spin $^{7}/_{2}$ quadrupolar nucleus with a high natural abundance (99.8%) and a relatively high gyromagnetic ratio, is commonly used to characterize numerous vanadium-containing systems, including polyoxovanadates, vanadium complexes, and vanadium-based catalysts.[43−45] For quadrupolar nuclei, the determination of the chemical shielding, the quadrupolar parameters, and the relative orientation of both tensors is crucial for safer line assignment.[46] For a series of ortho-, pyro-, and metavanadates containing mainly VO_4 (and few VO_5) vanadium sites, for instance, it has been demonstrated that the whole set of ^{51}V NMR parameters can be extracted from the simulation of the spectra.[46−52] It was then possible to draw useful correlations between the NMR and structural parameters, such as the vanadium coordination and the degree of polymerization of VO_n units.[43,48,49,51,52] However, for polyoxovanadate species exhibiting VO_5 and/or VO_6 coordination, the relationships between the structural units and the NMR parameters are much more difficult to establish.[53,54]

In this context, this paper shows that a methodology combining existing X-ray data, GIPAW calculations of ^{51}V NMR parameters, and NMR experiments can lead to a complete crystal structure determination of a decavanadate cluster, namely $Cs_4[H_2V_{10}O_{28}]\cdot 4H_2O$. This polyoxometalate (POM) has been extensively studied, due to its important role in various catalytic reactions,[55−57] biological processes,[58−61] and materials science.[62−65] However, despite the fact that several decavanadates have previously been characterized by ^{51}V NMR spectroscopy in the solid state,[43,53,54,66] the complete assignment of ^{51}V NMR lines has never been proposed, and the locations of protonation sites are still under investigation for various decavanadate structures.[67−75] Moreover, similar to other POMs, the decavanadate polyanion can be regarded as a model cluster of a metal oxide surface, for which the functionality and reactivity are determined by the nature and amount of OH ligands.[76] As a result, accurate characterizations of POM structures are also of interest for modeling catalytic reactions taking place at the metal oxide surfaces.

The detailed study of $Cs_4[H_2V_{10}O_{28}]\cdot 4H_2O$ opens new insights in the combination of first-principles methods and solid-state NMR spectroscopy for structural purposes. Indeed, the GIPAW/NMR approach presented in this contribution is original with regard to both the general calculation methodology aspects and the interpretation of ^{1}H/^{51}V parameters for hybrid POMs, considering the following key points.

(i) For the first time the *systematic theoretical* errors related to the GIPAW approach are evaluated using a benchmark of vanadium oxide systems. These errors will be of prime importance for accurate assignment of ^{51}V lines based on a statistical modeling of the data. To the best of our knowledge, DFT theoretical errors within the GIPAW method framework have rarely been discussed in the literature.

(ii) The GIPAW approach is validated here in the case of hybrid metal oxide structures, including protons and heavy nuclei such as ^{51}V and ^{133}Cs. Such systems exhibiting both light and heavy nuclei have been rarely reported in the literature.[77]

(iii) As frequently mentioned in the literature, ^{1}H chemical shifts are highly sensitive to H-bond networks, especially in organic systems containing C, N, O, and P atoms. This statement is extended here to vanadium derived oxides. Moreover, a clear distinction is made for OH/H_2O groups in terms of ^{1}H calculated CSA parameters. This observation is crucial, as OH/H_2O moieties in crystalline POMs could mimic—in a sense—the noncovalent binding between organic and inorganic entities in hybrid systems.

(32) Gervais, C.; Laurencin, D.; Wong, A.; Pourpoint, F.; Labram, J.; Woodward, B.; Howes, A. P.; Pike, K. J.; Dupree, R.; Mauri, F.; Bonhomme, C.; Smith, M. E. *Chem. Phys. Lett.* **2008**, *464*, 42–48.
(33) Bryce, D. L.; Bultz, E. B.; Aebi, D. *J. Am. Chem. Soc.* **2008**, *130*, 9282–9292.
(34) Profeta, M.; Benoit, M.; Mauri, F.; Pickard, C. J. *J. Am. Chem. Soc.* **2004**, *126*, 12628–12635.
(35) Truflandier, L.; Paris, M.; Boucher, F. *Phys. Rev. B* **2007**, *76*, 035102–17.
(36) Bühl, M. *Chem. Phys. Lett.* **1997**, *267*, 251–257.
(37) Bühl, M.; Hamprecht, F. A. *J. Comput. Chem.* **1998**, *19*, 113–122.
(38) Godbout, N.; Oldfield, E. *J. Am. Chem. Soc.* **1997**, *119*, 8065–8069.
(39) Bühl, M. *Magn. Reson. Chem.* **2006**, *44*, 661–668.
(40) Wilson, P. J.; Amos, R. D.; Handy, N. C. *Phys. Chem. Chem. Phys.* **2000**, *2*, 187–194.
(41) Schreckenbach, G. *J. Chem. Phys.* **1999**, *110*, 11936–11949.
(42) Bühl, *M.* Academic Press, 2008; Vol. Volume 64, p. 77−126.
(43) Lapina, O.; Khabibulin, D.; Shubin, A.; Terskikh, V. *Prog. Nucl. Magn. Reson. Spectrosc.* **2008**, *53*, 128–191.
(44) Lapina, O. B.; Mastikhin, V. M.; Shubin, A. A.; Krasilnikov, V. N.; Zamaraev, K. I. *Prog. Nucl. Magn. Reson. Spectrosc.* **1992**, *24*, 457–525.
(45) Lapina, O. B.; Shubin, A. A.; Khabibulin, D. F.; Terskikh, V. V.; Bodart, P. R.; Amoureux, J. *Catal. Today* **2003**, *78*, 91–104.
(46) Skibsted, J.; Nielsen, N. C.; Bildsoe, H.; Jakobsen, H. J. *J. Am. Chem. Soc.* **1993**, *115*, 7351–7362.
(47) Skibsted, J.; Nielsen, N. C.; Bildsøe, H.; Jakobsen, H. J. *Chem. Phys. Lett.* **1992**, *188*, 405–412.
(48) Nielsen, U. G.; Jakobsen, H. J.; Skibsted, J. *Inorg. Chem.* **2000**, *39*, 2135–2145.
(49) Hayakawa, S.; Yoko, T.; Sakka, S. *J. Solid State Chem.* **1994**, *112*, 329–339.
(50) Hansen, M. R.; Madsen, G. K. H.; Jakobsen, H. J.; Skibsted, J. *J. Phys. Chem. B* **2006**, *110*, 5975–5983.
(51) Nielsen, U. G.; Jakobsen, H. J.; Skibsted, J. *J. Phys. Chem B* **2001**, *105*, 420–429.
(52) Skibsted, J.; Jacobsen, C. J. H.; Jakobsen, H. J. *Inorg. Chem.* **1998**, *37*, 3083–3092.
(53) Durupthy, O.; Maquet, J.; Bonhomme, C.; Coradin, T.; Livage, J.; Steunou, N. *J. Mater. Chem.* **2008**, *18*, 3702–3712.
(54) Durupthy, O.; Jaber, M.; Steunou, N.; Maquet, J.; Chandrappa, G. T.; Livage, J. *Chem. Mater.* **2005**, *17*, 6395–6402.
(55) Malherbe, F.; Depège, C.; Forano, C.; Besse, J. P.; Atkins, M. P.; Sharma, B.; Wade, S. R. *Appl. Clay Sci.* **1998**, *13*, 451–466.
(56) Messmore, J. M.; Raines, R. T. *Arch. Biochem. Biophys.* **2000**, *381*, 25–30.
(57) Zhang, X.; Chen, X. *Inorg. Chem. Commun.* **2003**, *6*, 206–209.
(58) Crans, D. C.; Smee, J. J.; Gaidamauskas, E.; Yang, L. *Chem. Rev.* **2004**, *104*, 849–902.
(59) García-Vicente, S.; Yraola, F.; Marti, L.; González-Muñoz, E.; García-Barrado, M. J.; Cantó, C.; Abella, A.; Bour, S.; Artuch, R.; Sierra, C.; Brandi, N.; Carpéné, C.; Moratinos, J.; Camps, M.; Palacín, M.; Testar, X.; Gumà, A.; Albericio, F.; Royo, M.; Mian, A.; Zorzano, A. *Diabetes* **2007**, *56*, 486–493.
(60) Hua, S.; Inesi, G.; Toyoshima, C. *J. Biol. Chem.* **2000**, *275*, 30546–30550.
(61) Aureliano, M.; Crans, D. C. *J. Inorg. Biochem.* **2009**, *103*, 536–546.
(62) Crans, D. C.; Baruah, B.; Ross, A.; Levinger, N. E. *Coordin. Chem. Rev.* **2009**, *253*, 2178–2185.
(63) Mai, L.; Han, C. *Mater. Lett.* **2008**, *62*, 1458–1461.
(64) Carn, F.; Steunou, N.; Djabourov, M.; Coradin, T.; Ribot, F.; Livage, J. *Soft Matter* **2008**, *4*, 735–738.
(65) Carn, F.; Djabourov, M.; Coradin, T.; Livage, J.; Steunou, N. *J. Phys. Chem. B* **2008**, *112*, 12596–12605.
(66) Eckert, H.; Wachs, I. E. *J. Phys. Chem.* **1989**, *93*, 6796–6805.
(67) Lin, J.; Lu, J.; Cao, R.; Chen, J.; Su, C. *Dalton Trans.* **2009**, 1101–1103.
(68) Crans, D. C.; Mahroof-Tahir, M.; Anderson, O. P.; Miller, M. M. *Inorg. Chem.* **1994**, *33*, 5586–5590.
(69) Kumagai, H.; Arishima, M.; Kitagawa, S.; Ymada, K.; Kawata, S.; Kaizaki, S. *Inorg. Chem.* **2002**, *41*, 1989–1992.
(70) Schulz-Dobrick, M.; Jansen, M. *Inorg. Chem.* **2007**, *46*, 4380–4382.
(71) Correia, I.; Avecilla, F.; Marcao, S.; Pessoa, J. C. *Inorg. Chim. Acta* **2004**, *357*, 4476–4487.
(72) Ferreira da Silva, J. L.; Fátima Minas da Piedade, M.; Teresa Duarte, M. *Inorg. Chim. Acta* **2003**, *356*, 222–242.
(73) Nakamura, S.; Ozeki, T. *Dalton Trans.* **2001**, *4*, 472–480.
(74) Nakamura, S.; Ozeki, T. *Dalton Trans.* **2008**, *44*, 6135–6140.
(75) Sarkar, A.; Pal, S. *Polyhedron* **2008**, *27*, 3472–3476.
(76) Gouzerh, P.; Proust, A. *Chem. Rev.* **1998**, *98*, 77–112.
(77) Laurencin, D.; Gervais, C.; Wong, A.; Coelho, C.; Mauri, F.; Massiot, D.; Smith, M. E.; Bonhomme, C. *J. Am. Chem. Soc.* **2009**, *131*, 13430–13440.

(iv) The ^{51}V GIPAW data—including CSA and quadrupolar data—has led to accurate relationships between the NMR parameters and local distortions in VO_6 environments in terms of bond angles and interatomic distances. These relationships will be useful in interpreting NMR spectra of amorphous or crystalline polyoxovanadates and vanadium oxides containing VO_6 units. Moreover, it is shown that ^{51}V NMR parameters are extremely sensitive to hydrogen−oxygen bonding interactions, leading to the following paradox: in the case of $Cs_4[H_2V_{10}O_{28}].4H_2O$, the complex problem of proton location will be solved by careful analysis of experimental/calculated ^{51}V data, whereas the study of the corresponding ^{1}H parameters failed for that purpose.

The paper is organized as follows. Section 2 presents experimental and computational methods. In section 3, the underlying uncertainties of the theoretical approach used for the prediction of ^{51}V solid-state NMR parameters are accurately quantified and discussed. These results are important in supporting the ^{51}V resonance assignment of the magic angle spinning (MAS) spectra. In section 4, the X-ray centrosymmetric crystallographic structure of $Cs_4[H_2V_{10}O_{28}]\cdot 4H_2O$ is described. Considering the fact that protons are not located from the single-crystal XRD data, two possible isomers bearing different hydroxy ligands are considered. In section 5, the possible hydrogen concerted exchange between those isomers is discussed in terms of the energy barrier deduced from DFT calculations and ^{1}H solid-state NMR at various temperatures. In section 6, first-principles NMR calculations show that the structure of $Cs_4[H_2V_{10}O_{28}]\cdot 4H_2O$ consists of only one isomer for which the five isotropic ^{51}V resonances are fully assigned. The location of hydroxy ligands at the surface of the cluster is consequently unambiguously determined, and these results are consistent with ^{51}V 3QMAS NMR spectra recorded with and without ^{1}H decoupling. In addition, relationships between NMR parameters and VO_6 polyhedron deformations are established.

2. Materials and Methods

2.1. Sample Preparation. The $Cs_4[H_2V_{10}O_{28}]\cdot 4H_2O$ decavanadate cluster was prepared according to a previously reported chemical procedure.[53] The purity and crystallinity of this decavanadate compound was checked by means of X-ray diffraction and chemical analysis.

2.2. ^{51}V 3Q MAS NMR. Multiple quantum MAS (MQMAS) NMR experiments were performed on a Bruker AVANCE 400 spectrometer at 9.4 T and with a 4 mm zirconia rotor. ^{51}V 3-quantum (3Q) spectra were acquired with the multiplex soft pulse adding mixing (SPAM) MQMAS sequence.[78] The pulse durations of P1, P2, and P3 which depend on the quadrupolar interaction were optimized. The pulse sequence is presented in Figure 7b. For the spectra centered on −545 ppm, pulse durations of P1, P2, and P3 were 3.0, 1.25, and 10.5 μs, respectively. For the spectra centered on −430 ppm, pulse durations of P1, P2, and P3 were 1.5, 1.0, and 3.0 μs, respectively. For all spectra, the amplitude $\Omega_{RF}/2\pi$ of the radio frequency was 120 kHz for the two first pulses and 15 kHz for the third pulse. The multiplex spectra were recorded at the spinning rate $\nu_{Rot} = 14$ kHz, with a 0.25 s recycle delay, 71.42 μs for the increment of the t1 period with rotor synchronization, 30 sections, and 1200 accumulations. The power level for ^{1}H decoupling was 70 kHz. Data processing, shearing transformation, and scaling of the F1 axis were performed using "MSM" and "xfshear".[78]

2.3. ^{1}H MAS NMR. ^{1}H MAS NMR spectra were recorded on a Bruker Avance 500 spectrometer using a CP-MAS 4.0 mm Bruker probe. Solid samples were spun at 10 kHz using ZrO_2 rotors. A single $\pi/4$ pulse excitation of 2 μs was used. ^{1}H NMR spectra were acquired with a recycle delay of 5 s and an accumulation of eight transients. Isotropic chemical shifts were referenced to TMS.

2.4. Conventions and Numerical Simulations. The conventions used to calculate the shielding parameters $\{\sigma_{iso}, \Delta\sigma, \eta_\sigma\}$ from the shielding theoretical tensor eigenvalues $\{\sigma_{xx}, \sigma_{yy}, \sigma_{zz}\}$ are defined as follows.

Isotropic component:

$$\sigma_{iso} = \frac{1}{3}(\sigma_{xx} + \sigma_{yy} + \sigma_{zz}) \quad (1)$$

Anisotropic component:

$$\Delta\sigma = \sigma_{iso} - \sigma_{zz} \quad (2)$$

Asymmetry component:

$$\eta_\sigma = (\sigma_{xx} - \sigma_{yy})/\Delta\sigma \quad (3)$$

With

$$|\sigma_{zz} - \sigma_{iso}| \geq |\sigma_{xx} - \sigma_{iso}| \geq |\sigma_{yy} - \sigma_{iso}| \quad (4)$$

The experimental chemical shift parameters $\{\delta_{iso}, \Delta\delta, \eta_\delta\}$ are calculated using relations similar to (1), (2), and (3). The asymmetry and anisotropy of chemical shifts are related to the shielding parameters by $\Delta\delta = -\Delta\sigma$ and $\eta_\delta = \eta_\sigma$, whereas the isotropic chemical shift is defined with respect to a reference value generally obtained from liquid state measurements:

$$\delta_{iso} = -(\sigma_{iso} - \sigma_{ref}) \quad (5)$$

Unfortunately, first-principles calculations of σ_{ref} involve the consideration of vibrational and solvent effects. In order to circumvent such difficult calculations, σ_{ref} was evaluated by assuming a linear regression between computed σ_{iso} and the experimental values of δ_{iso}.[35]

The theoretical quadrupole coupling constant (C_q) and asymmetry parameter (η_q) are defined from the calculated V_{ii} eigenvalues of the electric field gradient tensor (EFG) as follows:

$$C_q = eQV_{zz}/h \quad (6)$$

$$\eta_q = (V_{yy} - V_{xx})/V_{zz} \quad (7)$$

with

$$|V_{zz}| \geq |V_{xx}| \geq |V_{yy}| \quad (8)$$

The theoretical eigenvalues of the traceless quadrupolar coupling tensor (**Q**) can also be computed using a generalization of eq 6, which is

$$Q_{ii} = eQV_{ii}/h \quad (9)$$

where e, h, and Q are the electronic charge, the Planck constant, and the quadrupolar momentum, respectively. For the last item, we have used a value of 51 mbarn (see section 3 for details). Conversely, the experimental eigenvalues of Q can be recovered from the experimental quadrupolar parameters using the following set of equations:

$$Q_{zz} = C_q \quad (10)$$

$$Q_{xx} = -\frac{1}{2}(1 + \eta_q)C_q \quad (11)$$

$$Q_{yy} = -\frac{1}{2}(1 - \eta_q)C_q \quad (12)$$

The orientation of the shielding tensor in the EFG tensor principal axis system (PAS) is described by the set of Euler angles $\{\psi, \chi,$

(78) Malicki, N.; Mafra, L.; Quoineaud, A. A.; Rocha, J.; Thibault-Starzyk, F.; Fernandez, C. *Solid State Nucl. Magn. Reson.* **2005**, *28*, 13–21.

$\xi\}$ using the Rose conventions.[79] When NMR experiments were recorded on powder samples, 16 sets of Euler angles led to identical spectra. Here, the definition interval of the Euler angles was narrowed down to $0 \leq \psi \leq \pi$ and $0 \leq \{\chi, \xi\} \leq \pi/2$, in order to obtain a unique defined set of Euler angles.[47] Experimentally, this set of angles can be estimated through careful analysis of both isotropic lines and spinning sidebands. Unfortunately, in this work, we were not able to determine with accuracy these parameters due to the low values of the anisotropy parameters. As a result, $\{\psi, \chi, \xi\}$ were estimated to be close to $\{0, 0, \pi/2\}$. Numerical simulations of the ^{51}V MAS NMR spectra were performed with the DMFIT program including the QUASAR extension.[80,81] These simulations included the effects of the chemical shift anisotropy, as well as first- and second-order quadrupolar interactions. Both central and satellite transitions were considered with a number of 40 spinning side bands (SSBs) provided by DMFIT. Some simulations were confirmed by using the SIMPSON simulation package.[82]

2.5. Computational Details. Periodic first-principles calculations were carried out at the DFT level of theory using the generalized gradient approximation (GGA) of the exchange-correlation potential proposed by Perdew and Wang (PW91),[83,84] in conjunction with pseudopotential to treat the interactions of the nuclei and core states with valence electrons, and plane-wave (PW) basis set. The all-electron EFG tensors were calculated using the PAW approach developed by Blöchl et al.,[29,30] along with the GIPAW method introduced by Pickard et al. to compute the shielding tensor.[31,85] Both approaches are implemented in the CASTEP code.[86] In order to achieve the full convergence and use moderate computational resources, the so-called "ultrasoft" pseudopotentials (USPP) were used.[87] The selection of core states for O and Cs were 1s and [Kr]4d, respectively. We have used two projectors to describe the 2s and 2p valence states of oxygen, one projector for the 5s and 6s states and two projectors for the 5p states of cesium. The core radii beyond which the pseudo wave functions match the all-electron ones were set to 1.3 and 3.9 bohr for O and Cs, respectively. Hydrogen pseudopotential was generated using two projectors for the 1s valence shell with a core radius of 0.8 bohr. As previously demonstrated, the inclusion of semicore atomic functions into the valence is required to obtain accurate and converged values for the ^{51}V shielding parameters,[35] using a core radius of 2.0 bohr, one projector for the 3s state, and two projectors per remaining channel. For the DFT geometry optimizations, the same USPP settings were used. Optimization of all—or part of—the atomic positions was performed by maintaining the experimental cell parameters and minimizing the forces down to the residual value of 0.05 eV/Å. All calculations were converged with respect to the kinetic energy cutoff used for the PW basis set expansion and to the *k*-point density needed for the Brillouin zone integration. A cutoff of 700 eV (51.5 Ry) along with a $2 \times 1 \times 2$ Monkhorst−Pack *k*-point grid[88] was sufficient to achieve convergence.

3. Theoretical ^{51}V NMR Parameter: Accuracy Evaluation

The evaluation of the DFT accuracy to predict physical observables is still a difficult task and a subject to a great deal of research. The evaluation of the accuracy of the (GI)PAW methods for predicting NMR parameters, especially for ^{51}V, remains unknown because three main sources of uncertainty have to be taken into account: (i) the quality of the structure, (ii) the functional used to approximate the exchange-correlation potential, and (iii) the reliability of the pseudopotentials. In the first case, the reader may find discussions about the influence of the structure quality on the calculated NMR parameters in several reviews.[22,23,28] In both of the last two cases, the influence of the pseudopotential and the exchange-correlation functional on the convergence and the accuracy of the calculated ^{51}V shielding and chemical shift parameters have also been reported.[35] Note that the influence of the structure quality upon the ^{51}V quadrupolar parameters have been extensively studied for the $AlVO_4$ compound.[50,89,90] Here, the main purpose is to evaluate the systematic theoretical errors of the method in order to obtain a reliable assignment of the ^{51}V resonances, which involves a statistical modeling of the data (see section 6.1 and the minimization of the χ^2 function). The theoretical errors concern all the NMR parameters except the Euler angles.

In order to evaluate the accuracy of the (GI)PAW methods, ^{51}V EFG and shielding parameters have been calculated for a benchmark of 11 vanadium-oxide systems (for a total of 14 vanadium nonequivalent sites). This benchmark along with the theoretical and experimental ^{51}V NMR parameters are presented in Tables S1 and S2 of the Supporting Information. In order to provide a correct analysis of the results, only structures well-resolved by XRD have been considered here. For this purpose, forces have been calculated by means of periodic DFT calculations for each experimental geometry: systems showing forces above a threshold of 0.7 eV/Å have been excluded (see Tables S1 and S2).

Regressions between the experimental and theoretical quadrupolar parameters obtained from XRD and DFT-optimized structures are plotted in Figures 1a,d, respectively. In this case, we made the choice to consider the entire sets of the eigenvalues provided by the theoretical EFG tensors. The theoretical quadrupole coupling constants and the quadrupolar asymmetry parameters derived from the set of eqs 10−12 are compiled in Tables S1 and S2. As shown in Figures 1a,d, the correlation between experimental and theoretical results is excellent over the complete range of compounds for both the XRD and DFT-optimized structures. These correlations allow the evaluation of the nuclear quadrupolar moment *Q* using eq 9, which is 51 ± 1 and 53 ± 1 mbarn for XRD and DFT-optimized structures, respectively. These results are in agreement with the experimental value of 51 ± 10 mbarn.[91] Finally, from the standard error calculated for the quadrupolar tensor eigenvalues it is possible to evaluate a theoretical uncertainty of ± 400 kHz for the quadrupolar constant and ± 0.2 for the asymmetry parameter.

Correlations of the experimental isotropic and anisotropy parameters with the theoretical results obtained from XRD and DFT-optimized structures (relaxation of the atomic positions within the experimental cell parameters) are plotted in Figure

(79) Rose, M. *Elementary Theory of Angular Momentum*; Dover Publications: Mineola, NY, 1995.
(80) Massiot, D.; Fayon, F.; Capron, M.; King, I.; Calvé, S. L.; Alonso, B.; Durand, J.; Bujoli, B.; Gan, Z.; Hoatson, G. *Magn. Reson. Chem.* **2002**, *40*, 70–76.
(81) Amoureux, J.; Fernandez, C. QUASAR Solid State NMR Simulation for Quadrupolar Nuclei; University of Lille, Lille, France, 2004 (this program is accessible within Dmfit).
(82) Bak, M.; Rasmussen, J. T.; Nielsen, N. C. *J. Magn. Reson.* **2000**, *147*, 296–330.
(83) Perdew, J. P.; Wang, Y. *Phys. Rev. B* **1992**, *45*, 13244.
(84) Perdew, J. P.; Chevary, J. A.; Vosko, S. H.; Jackson, K. A.; Pederson, M. R.; Singh, D. J.; Fiolhais, C. *Phys. Rev. B* **1992**, *46*, 6671.
(85) Yates, J. R.; Pickard, C. J.; Mauri, F. *Phys. Rev. B* **2007**, *76*, 024401–11.
(86) Segall, M. D.; Lindan, P. J. D.; Probert, M. J.; Pickard, C. J.; Hasnip, P. J.; Clark, S. J.; Payne, M. C. *J. Phys.: Condens. Matter* **2002**, *14*, 2717–2744.
(87) Vanderbilt, D. *Phys. Rev. B* **1990**, *41*, 7892.
(88) Monkhorst, H. J.; Pack, J. D. *Phys. Rev. B* **1976**, *13*, 5188.
(89) Gee, B. A. *Solid State Nucl. Magn. Reson.* **2006**, *30*, 171–181.
(90) Truflandier, L.; Paris, M.; Payen, C.; Boucher, F. *J. Phys. Chem. B* **2006**, *110*, 21403–21407.
(91) Childs, W. J. *Phys. Rev.* **1967**, *156*, 71.

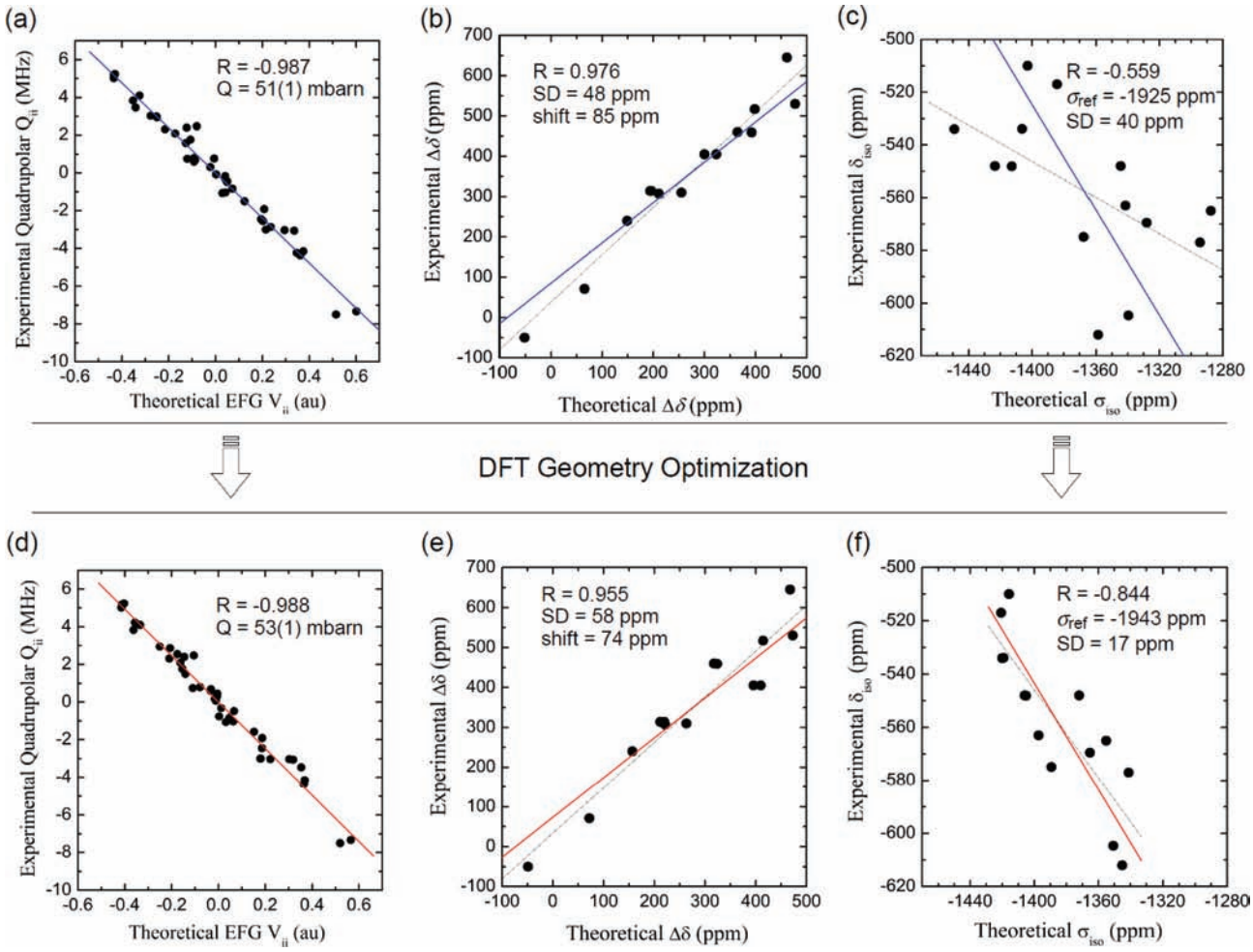

Figure 1. Correlations between experimental and theoretical ^{51}V NMR parameters for XRD and DFT-optimized structures obtained for a benchmark of 11 vanadate compounds described in Tables S1 and S2 of the Supporting Information: (a, d) experimental quadrupolar tensors eigenvalues vs theoretical electric field gradient eigenvalues (the quadrupolar moment Q is calculated using the relation (9); (b, e) experimental vs theoretical anisotropy parameters (shift and SD stand for the plot intercept and the standard deviation, respectively); (c, f) experimental chemical shift vs theoretical isotropic shielding (σ_{ref} is the plot intercept; unconstrained fits obtained are also reported using dashed lines).

1 respectively. For obvious reasons, the slope of the linear fits was set to 1 (freely fitted slopes are also reported the figures). Concerning the anisotropy parameter, comparison of both regressions clearly indicates that geometry optimization does not improve the agreement between both sets of data. In that case, if one compares the correlation coefficients of 0.98 and 0.96 obtained for the XRD and DFT geometries, respectively, it appears that the results are slightly less accurate for optimized structures. Nevertheless, it is worth noting that if the structures obtained from poorly resolved XRD data are taken into account (those with forces >0.7 eV/Å in Tables S1 and S2), the geometry optimization will undoubtedly improve the theoretical accuracy.[22] However, in this case, it is well-known that the intrinsic error of the exchange-correlation functional used during the DFT geometry relaxation process is responsible for the overestimated bond lengths.

Second, we have observed that the theoretical anisotropies are systematically underestimated with a shift of about 80 ppm; the standard deviation is found to be around 50 ppm. The correlations for the theoretical isotropic shieldings vs experimental chemical shifts are presented in Figure 1c,f. Considering DFT-optimized geometries, it was shown that the deviation between theory and experiment is around 17 ppm, whereas theoretical values obtained from XRD structures reach a mean discrepancy of 40 ppm. Overall, these results demonstrate that the error introduced by DFT through the structure relaxation is less significant than the uncertainties of the powder XRD data. At first glance, the theoretical deviations obtained for the ^{51}V chemical shifts might not be sufficient to accurately distinguish nonequivalent vanadium sites in vanadium oxide compounds, considering the short range of variation—less than 120 ppm here. Despite these limitations, assignment of ^{51}V resonances in structures presenting several nonequivalent sites can be safely carried out by adjusting the value of σ_{ref}, i.e., by using one of the calculated isotropic shielding as a reference value. This method has been successfully applied for the assignment of the ^{51}V chemical shifts in the α-$Mg_2V_2O_7$, β-$Mg_2V_2O_7$, CaV_2O_7,[35] and $AlVO_4$ compounds.[90]

To conclude, the use of GGA-PW91 functional for predicting ^{51}V NMR parameters led to the following mean deviations compared to experiment: (i) ±40 and ±17 ppm for the chemical shift (δ_{iso}) obtained from XRD and DFT-optimized structures, respectively; (ii) a constant shift of −85 ppm for the chemical shift anisotropy ($\Delta\delta$) and standard deviations of ±48 and ±58 ppm obtained from XRD and DFT-optimized structures, respectively; (iii) ±400 kHz for the quadrupolar constant (C_q), for both XRD and DFT-optimized structures; (iv) mean deviations for the asymmetry parameters (η_δ and η_q) around ±0.2. It

Table 1. Main XRD Data and Structural Parameters of $Cs_4[H_2V_{10}O_{28}]\cdot 4H_2O$

	crystallographic structure	
	Rigotti et al.[a] (R-DVD)	Tatyanina et al.[b] (T-DVD)
crystal	*twinned* crystal	*single* crystal
T (K)	298	293
R factor	0.075	0.057
a (Å)	10.072(4)	10.084(2)
b (Å)	14.077(3)	14.129(2)
c (Å)	11.528(3)	11.553(2)
β (deg)	108.10(3)	108.21
O1···O2 (Å)	2.59(4)	2.612(8)
V−O dist range (Å)	1.56(2)−2.34(2)	1.600(8)−2.322(8)
Cs−O dist range (Å)	3.08(3)−3.41(2)	3.073(7)−3.446(7)
bond valence of O1	1.28	1.33
bond valence of O2	1.76	1.78
mean bond valence of the decavanadate oxygens	1.8 ± 0.2	1.9 ± 0.2

[a] From ref 92. [b] From ref. 93.

should be noted that the experimental uncertainties arising from spectral simulations have been found to be smaller, with ±1 ppm for δ_{iso}, ±10 ppm for $\Delta\delta$, ±100 kHz for C_q, and ±0.1 for η_δ and η_q.[53]

4. Structure of $Cs_4[H_2V_{10}O_{28}]\cdot 4H_2O$ and Problems

4.1. Description. The crystallographic structure of $Cs_4[H_2V_{10}O_{28}]\cdot 4H_2O$ was independently examined by Rigotti et al. and Tatyanina et al. by means of single-crystal XRD experiments. In the former case, a twinned crystal was considered.[92,93] In the rest of the paper, their structures are referred to as R-DVD and T-DVD, respectively, where decavanadate is denoted as DVD. The DVD structure is described in a centrosymmetric monoclinic $P2_1/c$ space group with a = 10.084(2) Å, b = 14.129(2) Å, c = 11.553(2) Å, β = 108.21(3)°, V = 1563.6(5) Å^3, and Z = 2 (the T-DVD cell parameters and distances are chosen for reference in the text, as this structural refinement presents the best accuracy; see Table 1). The structure of the decavanadate anion (Figure 2a) consists of an arrangement of 10 edge-shared VO_6 octahedra, with five nonequivalent vanadium atoms related to the others by the presence of a center of symmetry. These VO_6 octahedra show typical distortions of V(V) cations coordinated to oxo ligands, which are related to the mutual repulsion between the cations.[94] Three chemical types of vanadium centers (namely, a−c; see Figure 2a) can be distinguished by considering the binding modes of the oxo ligands: Va = V(μ_2-O)$_2$(μ_3-O)$_2$(μ_6-O)$_2$, Vb/Vb′ = VO(μ_2-O)$_4$(μ_6-O), Vc/Vc′ = VO(μ_2-O)$_2$(μ_3-O)$_2$(μ_6-O). The polyhedra around Cs cations are quite different and ill-defined in shape. Cs(1) is eight-coordinated to two water oxygens and six O atoms belonging to five distinct polyanions, while Cs(2) is coordinated to only one water oxygen and eight O atoms of three neighboring decavanadate clusters. Decavanadate polyanions are arranged in infinite layers parallel to the (100) plane and stacked along the [100] direction (see Figure 2b,c). The layers are joined together by ionic interactions with Cs(1) atoms and a hydrogen-bond network created by water molecules. Within these layers, the DVDs have ionic interaction with Cs(2) atoms, but each polyanion is also involved in four intermolecular O···O contacts (2.61 Å). which are all crystallographically equivalent (Figures 2b and 3a). These short intermolecular distances are a strong indication of hydrogen bonding between decavanadate species, despite the fact that protons could not be located from the X-ray diffraction maps. On the basis of these hydrogen-bond and V−O distances, the hydrogen atom is presumably located between the oxygen atoms O1 and O2 of the decavanadate cluster (see Figure 3a,b). Therefore, one can distinguish between two possible decavanadate isomers, where O1 and O2 act as either donors or acceptors of a hydrogen bond. At this stage, it follows that some uncertainty exists in whether the OH ligand is located on O1 or O2.

In order to locate the position of hydroxyl ligands at the surface of decavanadate clusters, empirical relations connecting bond length and bond valence are commonly employed using the exponential law proposed by Brown.[95] The most significant results obtained for both experimental structures are collected in Table 1. For each decavanadate polyanion (T-DVD and R-DVD), the bond valences of oxygen atoms range from 1.6 to 2.0, with the exception of oxygen O1, for which the value is 1.3. In comparison to the oxygen valence of 1.8 obtained for O2, this suggests that O1 is the protonation site. Despite this strong indication, this work aims at confirming these empirical results, because a dynamic exchange of a proton between O1 and O2 cannot be definitively ruled out from the X-ray diffraction and bond valence calculations.

From the ^{51}V NMR point of view, the direct observation of five resolved ^{51}V lines for $Cs_4[H_2V_{10}O_{28}]\cdot 4H_2O$ (see sections 6.1 and 6.2) demonstrates clearly the absence of proton exchange on the NMR time scale. All further calculations will be performed in order to confirm this fact and, most importantly, to locate precisely the intercluster proton.

4.2. Structural Quality and Investigation of the VO_6 Octahedral Distortions. In this section, the accuracy of the crystallographic structure and the degree of distortion of the VO_6 entities are discussed. The analysis tools introduced here will be useful in section 6.1 for interpreting the ^{51}V NMR resonance assignments, and in section 6.3, for the extraction of accurate correlations between the VO_6 octahedral deformations and the computed ^{51}V NMR parameters.

As pointed out in Table 1, the structural refinement obtained by Tatyanina et al. (T-DVD) shows a better accuracy than that obtained by Rigotti et al. (R-DVD). First, a difference in the reliability factors ($R_{T\text{-}DVD}$ = 0.057 and $R_{R\text{-}DVD}$ = 0.075) is observed and can be directly correlated to the fact that the R-DVD structure was obtained from a twinned crystal. Second, the estimated standard deviations (esd) of the refined atomic positions are at least 3 times larger for the R-DVD structure than for T-DVD.[92,93] Consequently, the esd's of the bond lengths are around 0.01 Å for the R-DVD compared to 0.001 Å for the T-DVD. Despite this lack of accuracy, cell parameters and bond distances of both structures are in reasonably good agreement (Table 1).

It is well-known that, for X-ray diffraction experiments, when heavy atoms—such as cesium—are present in the structure, accurate reflections in the X-ray diffraction maps are required to determine and refine the positions of light elements. As a result, in addition to hydrogen atoms, the positions of oxygens may not be accurately determined due to the twinning of the R-DVD crystals.

(92) Rigotti, G.; Rivero, B. E.; Castellano, E. E. *Acta Crystallogr., Sect. C* **1987**, *43*, 197–201.
(93) Tatyanina, I. V.; Sergienko, V. S.; Zabolotskikh, A. V.; Torchenkova, E. A. *Koord. Khim.* **1987**, *13*, 680–688.
(94) Zavalij, P. Y.; Whittingham, M. S. *Acta Crystallogr., Sect. B* **1999**, *55*, 627–663.
(95) Brown, I. D.; Altermatt, D. *Acta Crystallogr., Sect. B* **1985**, *41*, 244–247.

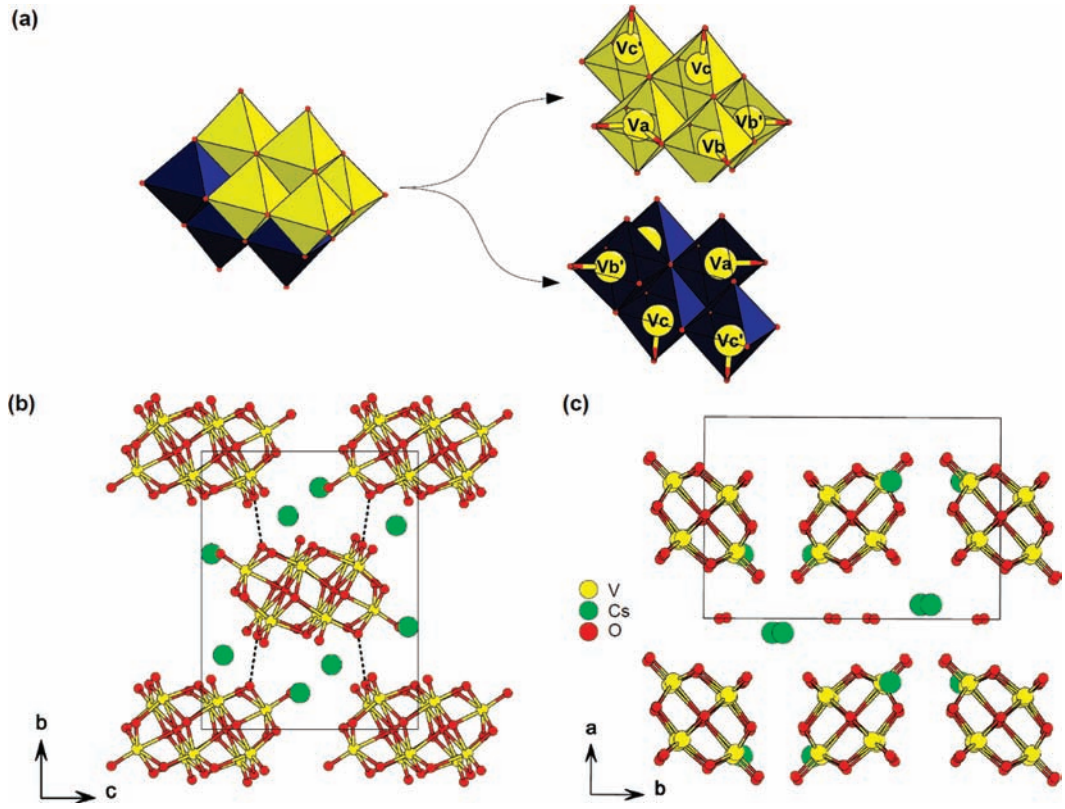

Figure 2. (a) Schematic representation of the nonequivalent vanadium sites of the $[V_{10}O_{28}]^{6-}$ polyanion. (b, c) Projections of the $Cs_4[H_2V_{10}O_{28}]\cdot 4H_2O$ structure along the [100] and [001] directions, respectively.

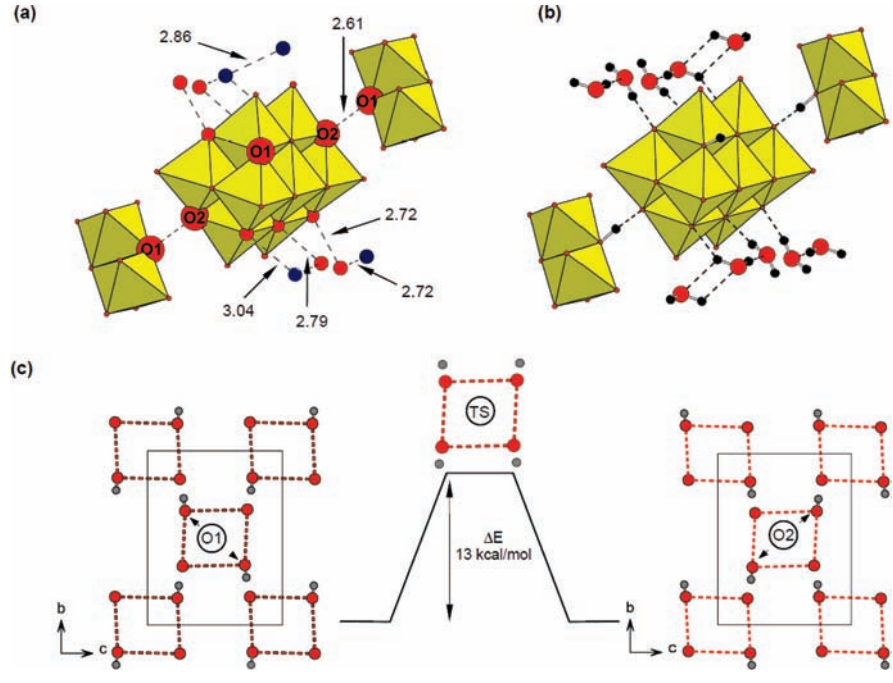

Figure 3. (a) Analysis of the interatomic distances (in Å) of $Cs_4[H_2V_{10}O_{28}]\cdot 4H_2O$ allowing the building up of the hydrogen-bond network involving OH ligands and water molecules. Crystallographic nonequivalent water oxygens are depicted in blue and red. (b) Possible geometry with the intercluster proton linked to O1. (c) Schematic representation of the possible proton transfer between the limit DFT-optimized structures O1-DVD and O2-DVD through the transition state TS-DVD.

The three chemical types of vanadium sites were previously identified considering the binding modes of the oxo ligands. These sites can also be distinguished considering the site distortion by focusing on bond lengths and angles. Because of the presence of a short vanadyl V═O bond (1.6 Å) and the longest V−O bond in the trans position (2.3 Å), the Vb and Vc octahedra are particularly distorted along the reference axis defined by the vanadyl bond (Figure 4a). The Va sites that are linked to two μ_6-O ligands are also highly distorted with the existence of two short V−O bonds (less than 1.7 Å). As shown

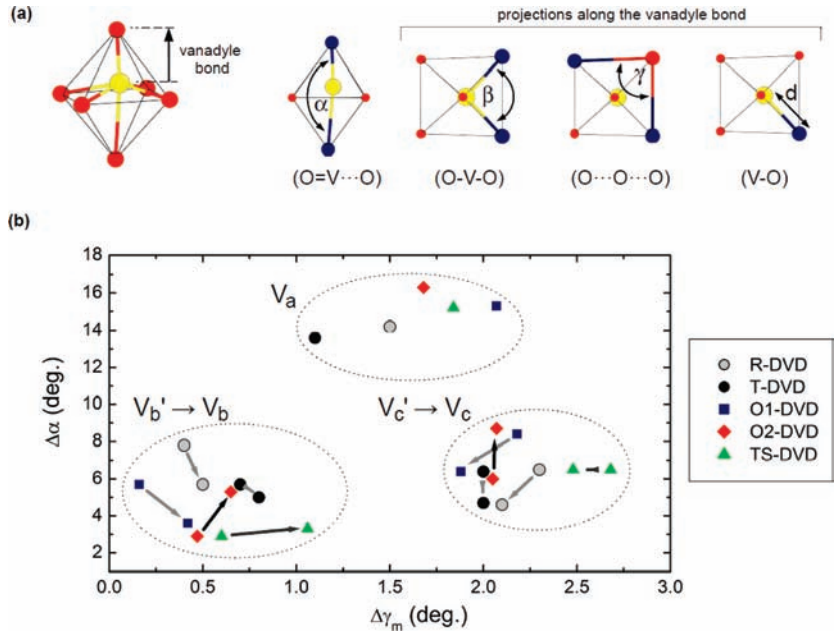

Figure 4. (a) Selected geometric parameters describing the VO_6 distortions in the $[V_{10}O_{28}]^{6-}$ polyanion. (b) Plot of the absolute deviation from 180° of α (noticed Δα) as a function of the mean absolute deviation $\Delta\gamma_m = {}^1/_4\sum_{i=1}^{4}|\gamma_i - 90|$ of the angle γ, for each vanadium site in the R-, T-, O1-, O2-, and TS-DVD structures.

in Figure 4a, various parameters could be used to evaluate the site distortion: (i) Δα, the deviation from 180° of the O═V···O angle taken along the reference axis, (ii) $\Delta\gamma_m = {}^1/_4\sum_{i=1}^{4}|\gamma_i - 90|$, the mean absolute deviation from 90° of the O···O···O angles defining the square plan orthogonal to the reference axis, or (iii) $\Delta\beta_m = {}^1/_4\sum_{i=1}^{4}|\beta_i - 90|$, the mean absolute deviation from 90° of the angle O−V−O. The reference axis is defined along the shortest V−O distance in the case of the Va site. As depicted in Figure 4b, the two crystallographic structures (R-DVD and T-DVD) are not equivalent in terms of VO_6 distortions. The graph representing Δα as a function of $\Delta\gamma_m$ can be decomposed into three areas related to the different vanadium sites (Va, Vb, and Vc) of the decavanadate polyanion. In particular, Figure 4b shows that the Va sites are characterized by a high deviation of α from 180°. For low values of Δα, the $\Delta\gamma_m$ values are split into two groups corresponding to the Vb/Vb′ and Vc/Vc′ sites. The comparison of VO_6 deformations from the R- and T-DVD structures shows that the VO_6 octahedra are more distorted in the structure resolved by Rigotti et al. Moreover, the geometries of the nonequivalent vanadium sites Vb (Vc) and Vb′ (Vc′) are closer in the T-DVD structure. It should be noticed that the same graph can be obtained if the mean absolute deviation $\Delta\beta_m$ is plotted as a function of $\Delta\gamma_m$.

5. Investigation of a Possible Concerted Proton Transfer

5.1. Geometry Optimizations and Energy Barrier Evaluation. In order to compute ^{51}V NMR parameters and determine whether the hydroxyl ligand is located on O1 or O2, the missing hydrogen atoms have been placed in the structure, and their positions optimized. For the water molecules, the initial orientation of the H_2O groups was defined by generating a realistic hydrogen bond network around the polyanion. The latter was deduced from structural topology by considering the symmetry constraints between the H_2O molecules. First, the eight water molecules of the unit cell, which are related through an inversion center ($Z = 2$), are located on the Wyckoff 4e position in the space group $P2_1/c$. Consequently, the hydrogen atoms have been placed in such a way of keeping the site-symmetry imposed by the oxygen atoms. Moreover, only water molecules with O···O distances around 2.7 and 3.0 Å (see Figure 3a) which are compatible with hydrogen bond lengths were retained, allowing us to decrease the number of possible isomers to only one configuration.

In order to determine the location of the OH ligand in DVD, we have defined and optimized five structural models—using the symmetry constraints—which cover the whole range of possibilities. First, for the crystallographic structures of $Cs_4[H_2V_{10}O_{28}]\cdot 4H_2O$ reported independently by Rigotti et al. and Tatyanina et al., a partial DFT geometry optimization was performed by maintaining all of the experimental parameters (the cell and the atomic coordinates of vanadium, cesium, and oxygen atoms) and relaxing only the atomic positions of the hydrogen atoms (OH ligands and H_2O molecules). These optimized structures are still labeled R-DVD and T-DVD, as the only difference from the original structures is the presence of protons. For these two cases, the starting configurations were built by considering that the OH ligand is located on the oxygen O1. We have also tried to optimize the T-DVD structure using a different starting configuration, where the OH ligand is located on the O2 oxygen. Even with drastic convergence criteria on the calculated forces, the OH ligand goes back "naturally" to the O1 site. This demonstrates that the potential energy surface (PES) related to the single-crystal XRD structure—keeping the $Cs_4[H_2V_{10}O_{28}]$ block fixed in the periodic cell—presents a single global minimum along the hydrogen transfer coordinate, which is reached for a bond length O1−H around 1.0 Å.

These results are in contrast with those deduced from the DFT structure relaxations where all the atomic positions—while keeping constant the experimental cell parameters—have been optimized. Three structures have been generated: (i) the first one (labeled as O1-DVD) was obtained with a starting geometry where the OH ligand on the decavanadate oxygen is located on O1 (O2 is the acceptor of the hydrogen bond); (ii) the second

one (labeled as O2-DVD) was obtained with a starting geometry where the OH ligand on the decavanadate oxygen is located on O2 (O1 is the acceptor of the hydrogen bond); (iii) the third one was obtained using equal O1···H and O2···H distances for the starting geometry and keeping frozen the intercluster hydrogen position in the unit cell during the relaxation process (labeled TS-DVD). We found that these three optimized structures are stationary points on the PES. Within the DFT accuracy, it appears that the O1-DVD and O2-DVD isomers are nearly isoenergetic, suggesting that the location of the proton on either O1 or O2 is equiprobable (see Table S3 in the Supporting Information). In comparison to the experimental R-DVD or T-DVD structures, slight differences of Vb/Vb′ and Vc/Vc′ octahedral distortions are observed for the optimized O1- and O2-DVD structures (Figure 4b). For the three fully optimized structures, the Va octahedral distortion is larger than the experimental distortion, both in the equatorial plane and along the shortest V−O distance. Figure 4b also shows that the proton transfer which would occur between O1- and O2-DVD induces a pseudoexchange of Vb′ with Vb and of Vc′ with Vc sites.

From a theoretical point of view, one can study the intercluster proton transfer between O1 and O2 thermodynamically, by considering the difference in free energy between product and reactant ($\Delta F°$), and kinetically, by considering the difference in free energy between the transition state and the reactant ($\Delta F^{\ddagger}$, which is related to the activation energy), with the formal equation:

$$\Delta F(T, g(\omega)) = \Delta E_{tot} + \Delta E_{zp}(g(\omega)) - T\Delta S(T, g(\omega)) \quad (13)$$

where ΔF, ΔE_{tot}, ΔE_{zp}, and ΔS are respectively the differences in free energy, total energy, zero point energy, and entropy and T is the absolute temperature. The last two terms of the relation (13) are dependent on the vibrational modes ω. Because calculation of the phonon spectrum $g(\omega)$ of $Cs_4[H_2V_{10}O_{28}]\cdot 4H_2O$ is beyond the scope of this study, some reasonable approximations were used to evaluate $\Delta F°$ and $\Delta F^{\ddagger}$.[96] Since the intercluster hydrogen bonds parameters in TS-DVD were found to be around 1.2 Å for the O1···H and O2···H distances and 178° for the O1···H···O2 angle (see Table S3),[97] it appears that this intermediate structure can be used for the evaluation of the energy barrier related to the proton transfer. The calculated value of $\Delta F^{\ddagger} = 13$ kcal/mol is on the order of magnitude of energy barriers reported for interconversion processes of hydroxyurea−vanadate(V) complexes involving proton transfers between H_2O and OH or between the oxygen and the OH ligands.[98] However, for these complexes the proton-transfer processes are especially favorable when they are assisted by a water molecule from the second coordination sphere, but such a "catalytic" effect cannot exist in this decavanadate cluster. Here we emphasize that this value should be considered with caution, considering that GGA functionals are known to underestimate activation energies.[99]

Finally, on the basis of the results deduced from the fully optimized geometries, the DFT tends to show that two local minima—namely O1- and O2-DVD—connected by a transition state coexist along the hydrogen transfer coordinate, which is in contradiction with the global minimum observed for the partially optimized structure T-DVD. In order to determine whether a possible concerted proton exchange occurs in $Cs_4[H_2V_{10}O_{28}]\cdot 4H_2O$, ^{1}H MAS NMR experiments were recorded at various temperatures.

5.2. ^{1}H NMR: Variable-Temperature MAS Experiments and First-Principles Calculations. The ^{1}H MAS NMR spectra recorded at 252, 298, and 315 K display two resonances at 5.1 and 14.4 ppm (Figure 5). These two resonances are assigned to the water molecules and OH ligands, respectively. In the former case, the broadening of the resonance is correlated with the temperature increase due to the thermal activation of H_2O vibrational modes, whereas in the latter case, no modification of the sharp signal is observed. This result can be explained by either the absence of any proton exchange between O1 and O2 in this temperature range or a very fast H exchange on the time scale of NMR. Considering that five distinct lines are observed in the ^{51}V spectrum (see sections 6.1 and 6.2 for the ^{51}V 3QMAS NMR experiment), this supports a definite location of the OH protons, without any significant exchange on the NMR time scale.

Moreover, from a qualitative point of view, considering the ^{1}H NMR and the activation energy of 13 kcal/mol calculated previously, we can evaluate the constant rate of exchange by using the Eyring equation. The computed values of 7×10^3 and 30 Hz at 315 and 252 K, respectively, strongly indicate that—if such exchange occurs—the resolution of the OH ligand resonances should be modified accordingly. Nevertheless, this implies that the O1-DVD and O2-DVD isomers exhibit different ^{1}H NMR signatures.

^{1}H chemical shift parameters were calculated from the five structures (Table 2). Chemical shifts were determined with a reference value of 31.6 ppm (eq 5).[28] The H_2O hydrogen shielding parameters were calculated considering the mean of values obtained from the four nonequivalent atoms present in the unit cell. We note that OH/H_2O CSA parameters are clearly distinguished. From a qualitative point of view, and assuming that the observed spinning sidebands in Figure 5 are exclusively related to CSA effects, it is obvious that the CSA for OH groups is much smaller than for H_2O molecules, in good agreement with the GIPAW predictions. In Figure S3 in the Supporting Information, two simulations of ^{1}H spectra describing the effects induced by the variations of $\Delta\delta$ have been drawn. We observe that the theoretical results underestimate the experimental anisotropies. However, it should be mentioned that some residual dipolar coupling may contribute to the intensity of the spinning sidebands. Pure CSA contributions could be measured by implementing specific recoupling sequences under MAS, at variable magnetic fields and various MAS frequencies. This task is out of the scope of the present work.

For the OH ligand, a value close to the experimental one is found for the O1-, O2-, and T-DVD structures. However, for the R-DVD structure, the calculated chemical shift is 1 ppm too high, which might be related to the poor quality of the structural resolution. As expected, the transition state structure

(96) Despite the disparity in deformations, we can consider that the O1-, O2-, and TS-DVD structures have the same phonon densities of states and zero-point energies, allowing us to approximate eq 13 by $\Delta F^{\ddagger} \approx \Delta E_{tot}$. Thus, for the O1- and O2-DVD geometries which are isoenergetic isomers, we have $\Delta F° \approx 0$.

(97) Note that, in comparison to O1- and O2-DVD, the couples Vc′/Vc and Vb′/Vb in TS-DVD could be distinguished solely by their deformations in the equatorial plane.

(98) Vrček, I. V.; Birus, M.; Buhl, M. *Inorg. Chem.* **2007**, *46*, 1488–1501.

(99) Koch, W.; Holthausen, M. C. *A Chemist's Guide to Density Functional Theory*, 2nd ed.; Wiley-VCH: Weinheim, Germany, 2001.

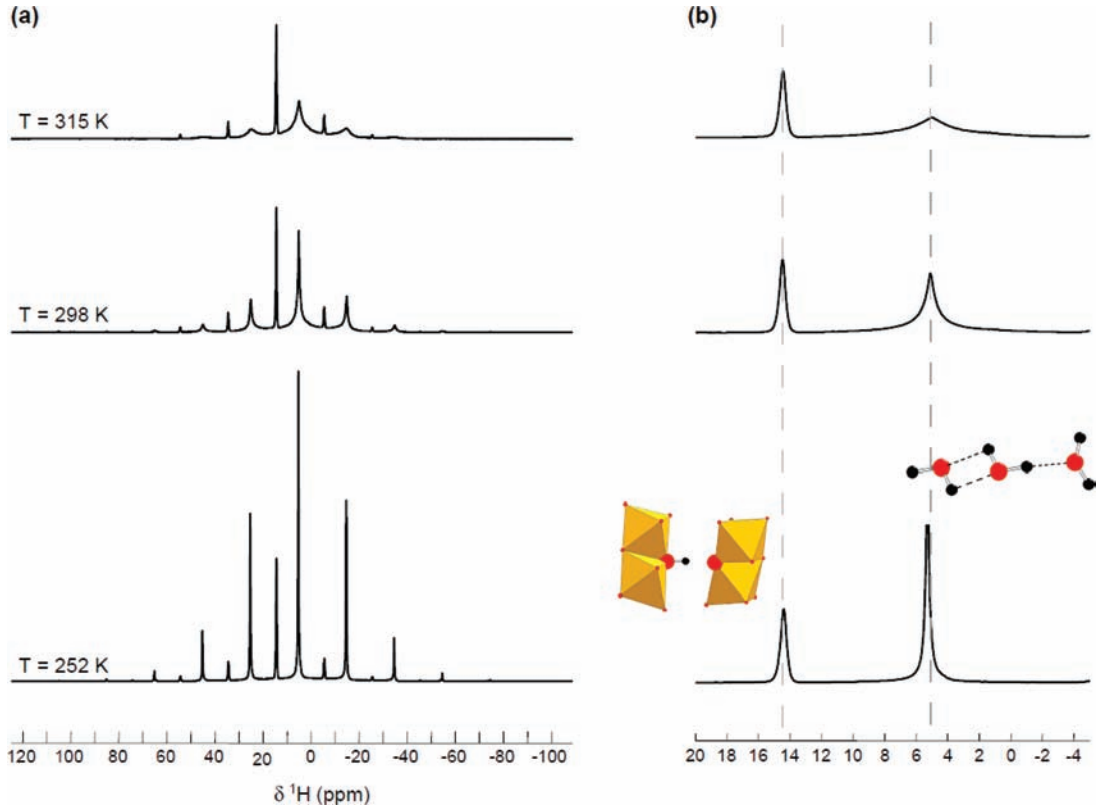

Figure 5. (a) ^{1}H MAS NMR spectrum of $Cs_4[H_2V_{10}O_{28}]\cdot 4HO$ spun at 10 kHz and recorded at different temperatures. (b) Magnification and assignment of the isotropic resonances in the experimental spectrum.

Table 2. Experimental and Calculated ^{1}H NMR Chemical Shift Parameters for $Cs_4[H_2V_{10}O_{28}]\cdot 4H_2O$

	H_2O^b			OH ligand		
structure	δ_{iso} (ppm)	$\Delta\delta$ (ppm)	η_δ	δ_{iso} (ppm)	$\Delta\delta$ (ppm)	η_δ
T-DVD	5.1	15.7	0.18	14.5	5.4	0.32
R-DVD	5.1	15.9	0.18	15.4	6.5	0.34
O1-DVD	5.2	15.9	0.19	14.6	6.1	0.23
O2-DVD	4.9	15.7	0.18	14.2	5.2	0.22
TS-DVD	4.8	15.6	0.18	20.5	7.1	0.16
exptl[a]	5.1			14.4		

[a] Only the isotropic component is reported. [b] Mean values from the four nonequivalent water hydrogen atoms.

is not the proper geometry to describe $Cs_4[H_2V_{10}O_{28}]\cdot 4H_2O$: the predicted value is too large by 6 ppm.

On the basis of the measured and calculated ^{1}H NMR chemical shifts, definitive conclusions about the concerted proton exchange cannot be drawn. Indeed, the ^{1}H chemical shifts of the O1H and O2H ligands are so similar that it is impossible to discriminate the corresponding resonances. Nevertheless, considering that the shape of the signal related to the intercluster proton is unmodified with respect to the temperature variation, we suspect that the two local minima deduced from the DFT optimizations together with the low energy barrier obtained for the transition state might arise from the exchange-correlation functional deficiency to accurately reproduce the PES. This remark is in contrast with the good performance usually observed for the GGA-PW91 functional to reproduce weak interactions in molecular systems—considering *post* Hartree−Fock methods as references.[100] But, as emphasized by Koch and Holthausen,[99] there is no general rule of thumb concerning the performance of an approximate exchange-correlation kernel unless a careful validation of the functional has been performed with regard to the class of the system under investigation. In order to identify the origin(s) of these subtle effects, an extended study of a set of protonated decavanadate clusters should be realized using accurate XRD and considering various exchange-correlation functionals. This will be addressed in a future work.

6. Experimental and Theoretical ^{51}V NMR Parameters

6.1. Resonance Assignment of $Cs_4[H_2V_{10}O_{28}]\cdot 4H_2O$. The experimental and calculated ^{51}V NMR parameters for the T-DVD, O1-DVD, and O2-DVD structures are compiled in Table 3, and the results obtained for the other structures (R-DVD and TS-DVD) are given in Table S4 of the Supporting Information. Theoretical ^{51}V isotropic chemical shifts of XRD and DFT-optimized models were determined with the reference values of $\sigma_{ref} = -1925$ and -1943 ppm, respectively (see section 3 and Figure 1c,f). From the two-dimensional correlations between measured and theoretical NMR parameters (C_q, δ_{iso}) presented in Figure 6, one can clearly observe that neither the XRD structure resolved by Rigotti et al. nor the DFT-optimized structure TS-DVD can assign the five experimental resonances. In the former case, the observed discrepancies are consistent with the poor quality of the X-ray data (see discussion in section 4.2). In the latter case, this corroborates the fact that the TS-DVD geometry, which is a stationary point between the O1-DVD and O2-DVD structures, is not energetically favorable and should be very close to the ideal transition state geometry found by the DFT. We notice that these results are in agreement with the analysis of the discrepancies observed for the ^{1}H chemical shifts (see discussion in section 5.2 and Table 2).

(100) Tsuzuki, S.; Luthi, H. P. *J. Chem. Phys.* **2001**, *114*, 3949–3957.

Table 3. Experimental and Calculated ^{51}V NMR Parameters for $Cs_4[H_2V_{10}O_{28}]\cdot 4H_2O$

expt	resonance	δ_{iso} (ppm)	$\Delta\delta$ (ppm)	η_δ	C_q (MHz)	η_q	Q_{cc}/C_q[a]	ψ (deg)	χ (deg)	ξ (deg)
^{51}V MAS[b]	5	−426	−340	0.3	6.4	0.4		0	0	90
	1	−518	−400	0.2	3.0	0.9		0	0	90
	2	−531	−450	0.4	2.2	0.4		0	0	90
	3	−540	−450	0.5	2.5	0.9		0	0	90
	4	−545	−450	0.2	4.0	0.5		0	0	90
^{51}V 3QMAS[c]	5	−427					8.0/7.8			
	1	−523					4.2/3.7			
	2	−536					2.1/2.0			
	3	−544					2.8/2.5			
	4	−550					4.4/4.2			

theory	site[d]	δ_{iso} (ppm)	$\Delta\delta$ (ppm)	η_δ	C_q (MHz)	η_q	ψ (deg)	χ (deg)	ξ (deg)
T-DVD	$a = 5$	−463	−292	0.35	6.4	0.52	67	9	66
	$b' = 1$	−484	−352	0.20	3.1	0.79	178	74	59
	$c = 2$	−523	−342	0.09	2.2	0.38	3	14	72
	$b = 3$	−537	−385	0.18	2.7	0.77	171	74	68
	$c' = 4$	−555	−359	0.14	4.2	0.75	66	23	26
	ΔP_i[e]	18	72	0.15	0.1	0.13			
O1-DVD	$a = 5$	−390	−289	0.42	7.7	0.48	165	12	38
	$b' \approx 1$	−520	−364	0.15	2.9	0.77	130	40	70
	$c \approx 2$	−523	−370	0.10	2.5	0.57	85	29	65
	$b \approx 3$	−527	−420	0.10	1.5	0.91	121	40	81
	$c' = 4$	−535	−358	0.08	4.4	0.52	133	23	49
	ΔP_i	14	58	0.20	0.6	0.08			
O2-DVD	$a = 5$	−397	−285	0.42	7.7	0.46	31	1	81
	$b' \approx 2$	−516	−387	0.18	1.7	0.24	5	73	39
	$c = 4$	−531	−358	0.12	4.7	0.56	56	21	53
	$b \approx 1$	−534	−394	0.04	2.4	0.97	170	33	79
	$c' \approx 3$	−528	−378	0.14	2.1	0.83	161	29	74
	ΔP_i	17	58	0.19	0.7	0.08			

[a] The Q_{cc} values are extracted by the simulation of ^{51}V 3QMAS spectra. C_q values are calculated from Q_{cc} values. [b] Values obtained from ref 53 [c] Values obtained from this work. [d] The experimental resonances 1−5 are assigned to vanadium sites {a, b, b′, c, c′} depicted in Figure 6a by minimizing the χ^2 function given in eq 14. When the assignment is unambiguous, the symbol = is used; otherwise the symbol ≈ is employed. [e] ΔP_i is the mean absolute deviation between the experimental and theoretical NMR parameter i, considering the five resonances.

The experimental ^{51}V resonances can be assigned by minimizing the function χ^2, where the variables are defined by the set of NMR parameters $\{\delta_{iso}, \Delta\delta, \eta, C_q, \eta_q\}$. We note here that the Euler angles have not been considered due to the lack of reliable experimental data (see section 2.4). As a result, the χ^2 function is defined as

$$x^2 = \frac{1}{n \times m - 1} \sum_i^n \sum_j^m \left\{ \frac{P_{ij}^{th} - P_{ij}^{exp}}{\Delta S_i^{th}} \right\}^2 \qquad (14)$$

where P^{th} and P^{exp} stand for the theoretical and experimental NMR parameters and ΔS^{th} denotes the respective theoretical standard deviations determined in section 3. The indices i and j run over the set of n observables and the m ^{51}V resonances, respectively. The χ^2 function takes into account only the DFT uncertainties by considering that the latter are much larger than those arising from the simulated experimental spectra. The best agreement is found for the experimental structure T-DVD with a χ^2 value of 0.9, compared to 1.5 for the DFT-optimized geometries O1- and O2-DVD, respectively. The corresponding assignments along with the mean-absolute deviations $\Delta P_i = 1/m\sum_j |P_{ij}^{th} - P_{ij}^{exp}|$ for each NMR parameter are collected in Table 3. From this table, we note that the ΔP_i values obtained for δ_{iso} are nearly the same for the three geometries. For the quadrupolar coupling constant a sizable discrepancy above 500 kHz is observed for O1- and O2-DVD, whereas this value is reduced to 100 kHz for the T-DVD structure. In the former cases, the worst values of χ^2 are mainly related to the strong deviations observed for C_q. This clearly demonstrates that the higher reliability is obtained for the T-DVD structure, for which an unambiguous assignment of the resonances to the five nonequivalent VO_6 octahedra can be proposed.

From the analysis of the ^{1}H NMR experiments (see section 5.2), and in agreement with the observation of five resolved ^{51}V lines, we have eliminated the possibility of a proton exchange, on an experimental basis only. As a result, considering the DFT-optimized structures, we observe from the two-dimensional correlations plotted in Figure 6 that only the resonances 5 and 4 can be assigned to the Va and Vc′ sites (or to the Va and Vc sites) if we consider the O1-DVD model (or O2-DVD). As expected, this demonstrates that the location of the intercluster proton on O1 or O2 cannot be realized, considering the fully relaxed structures. Only the good correlation between the experimental and theoretical NMR parameters obtained for the partially optimized experimental structure T-DVD shows that the OH ligand is located on O1, which is a bridging oxygen between Vb′ and Vc′.

Finally, we have shown that the assignment of all ^{51}V NMR signals is relevant to the possibility of distinguishing the optimized structures—taking care of the theoretical uncertainties—that differ from VO_6 polyhedral deformations—the heavy-atom positions—induced by the location of protons, revealing the remarkable sensitivity of ^{51}V NMR parameters on hydrogen−oxygen bonding interactions.

6.2. ^{51}V 3QMAS NMR: Probing the ^{51}V−^{1}H Proximities. In order to support the ^{51}V line assignment based on the computed NMR parameters of the T-DVD structure, ^{51}V 3QMAS NMR experiments were performed (the pulse sequence is resumed in

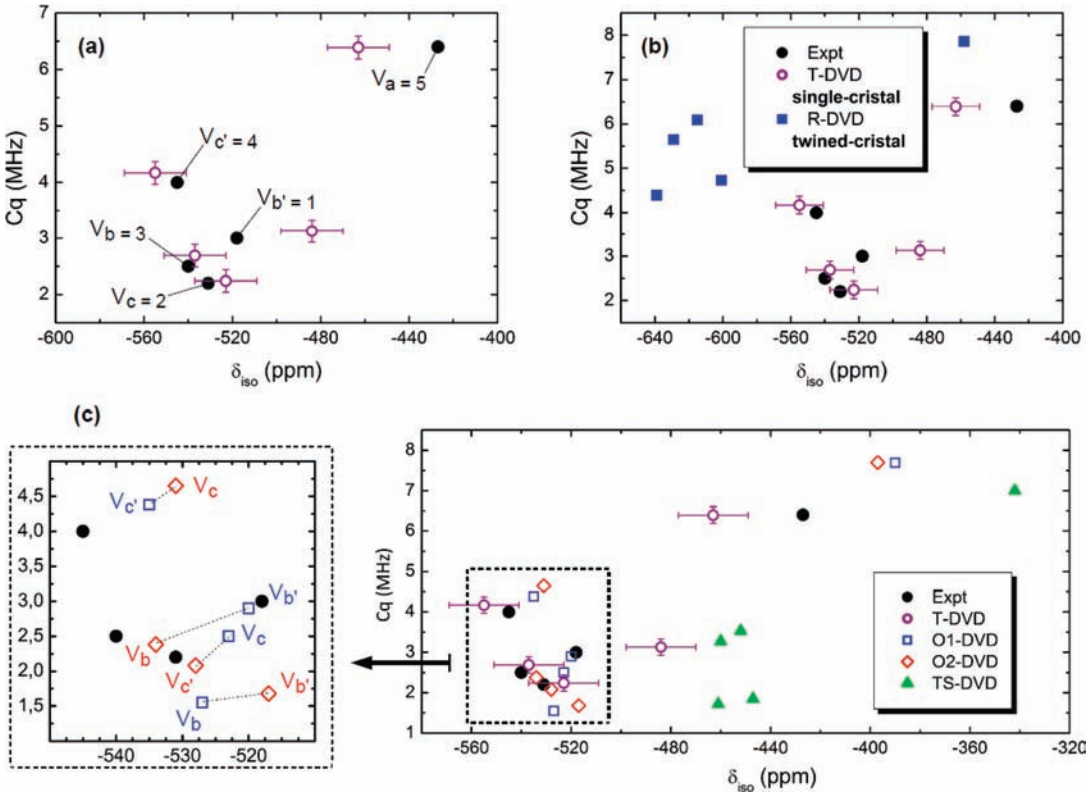

Figure 6. (a) δ_{iso} and C_q parameters for each vanadium site deduced from ^{51}V MAS experiments and DFT calculations. The unambiguous assignment of the experimental resonances based on calculated ^{51}V NMR parameters is obtained for the X-ray structure T-DVD. (b) Comparison of the experimental and calculated NMR parameters for the R-DVD and T-DVD structures, showing the low accuracy of the structure obtained from a twinned crystal. (c) Comparison of the calculated NMR parameters derived from DFT-optimized structures with experimental NMR parameters.

Figure 7b). This two-dimensional experiment correlates the evolution of the symmetrical ($^3/_2 \leftrightarrow -^3/_2$) triple-quantum transition with the evolution of the central transition under magic angle spinning to produce highly resolved isotropic NMR spectra. We have chosen to use a MQMAS sequence recently proposed by Malicki and co-workers,[78] which combines the multiplex phase cycling approach,[101] with the new soft pulse adding mixing method.[102] This new sequence increases the signal-to-noise ratio and allows recording 3Q, 5Q, and 7QMAS spectra within the same acquisition.[103]

Since the quadrupolar coupling constant of the ^{51}V NMR peak at −426 ppm is significantly larger than that of the other ^{51}V NMR signals, two 3QMAS NMR experiments have been recorded with different pulse lengths (see section 2.2) in order to obtain resolved signals in the regions close to −426 and −500 ppm (see Figures 7a and S1, respectively). One ^{51}V resolved signal at −427 ppm is clearly observed in the spectrum of Figure S1, while four broad resonances at −523, −536, −544, and −550 ppm are present in Figure 7a. The 3QMAS chemical shifts are fully consistent with those obtained by fitting ^{51}V MAS NMR spectra or DFT calculations (Table 3). The C_q and η_q parameters extracted by using line shape fitting of the anisotropic cross-section are in good agreement with calculated and experimental values of Table 3. However, we observe that for the signal at −426 ppm there is a large discrepancy between the calculated/1D-experimental C_q of Table 3 and the value extracted from 3QMAS. At this point, we presume that the quadrupolar coupling constant is overestimated by the multiple quantum experiment, considering that, in the ^{51}V MAS NMR spectrum, the shape of the quadrupolar line at −426 ppm has been safely characterized:[53] this value have been extracted from the simulation of the ^{51}V NMR spectra acquired at three different static magnetic fields (B_0 = 7.0, 9.4, and 14.0 T).

The observation of the ^{51}V line shapes in the two-dimensional contour plots shows a small distribution of chemical shifts and quadrupolar parameters for each signal. However, the four resonances of Figure 7a are characterized by a significant broadness resulting from residual ^{1}H−^{51}V dipolar coupling, which is not completely suppressed under high-speed MAS conditions. Knowing that the dipolar coupling is multiplied by the coherence order (three times for triple quantum),[104] one may expect significantly enhanced ^{1}H−^{51}V dipolar couplings during the triple quantum evolution, especially for VO_6 polyhedra covalently linked to protons. It has already been reported that significant resolution enhancement can be reached by applying continuous-wave decoupling or composite pulse decoupling for strongly coupled nuclei.[105] In the case of $Cs_4[H_2V_{10}O_{28}]\cdot 4H_2O$, a continuous-wave ^{1}H decoupling applied during the triple quantum evolution period provides a significant sharpening of the isotropic lines as shown in Figure 7c. It is worth noting that the line widths of the peaks at −518 ppm (Vb′ site) and −545 ppm (Vc′ site) are the most affected by ^{1}H decoupling, suggesting that these peaks are related to the vanadium sites which are covalently linked to a bridging OH ligand. As outlined in Figure 7, these results are fully consistent with the DFT calculations, which assign both signals to the Vb′ and Vc′ sites.

(101) Ivchenko, N.; Hughes, C. E.; Levitt, M. H. *J. Magn. Reson.* **2003**, *160*, 52–58.
(102) Gan, Z. H.; Kwak, H. T. *J. Magn. Reson.* **2004**, *168*, 346–351.
(103) Hajjar, R.; Millot, Y.; Man, P. P. *C. R. Chim.* **2008**, *11*, 380–386.
(104) Duer, M. J. *Chem. Phys. Lett.* **1997**, *277*, 167–174.
(105) Lacassagne, V.; Florian, P.; Montouillout, V.; Gervais, C.; Babonneau, F.; Massiot, D. *Magn. Reson. Chem.* **1998**, *36*, 956–959.

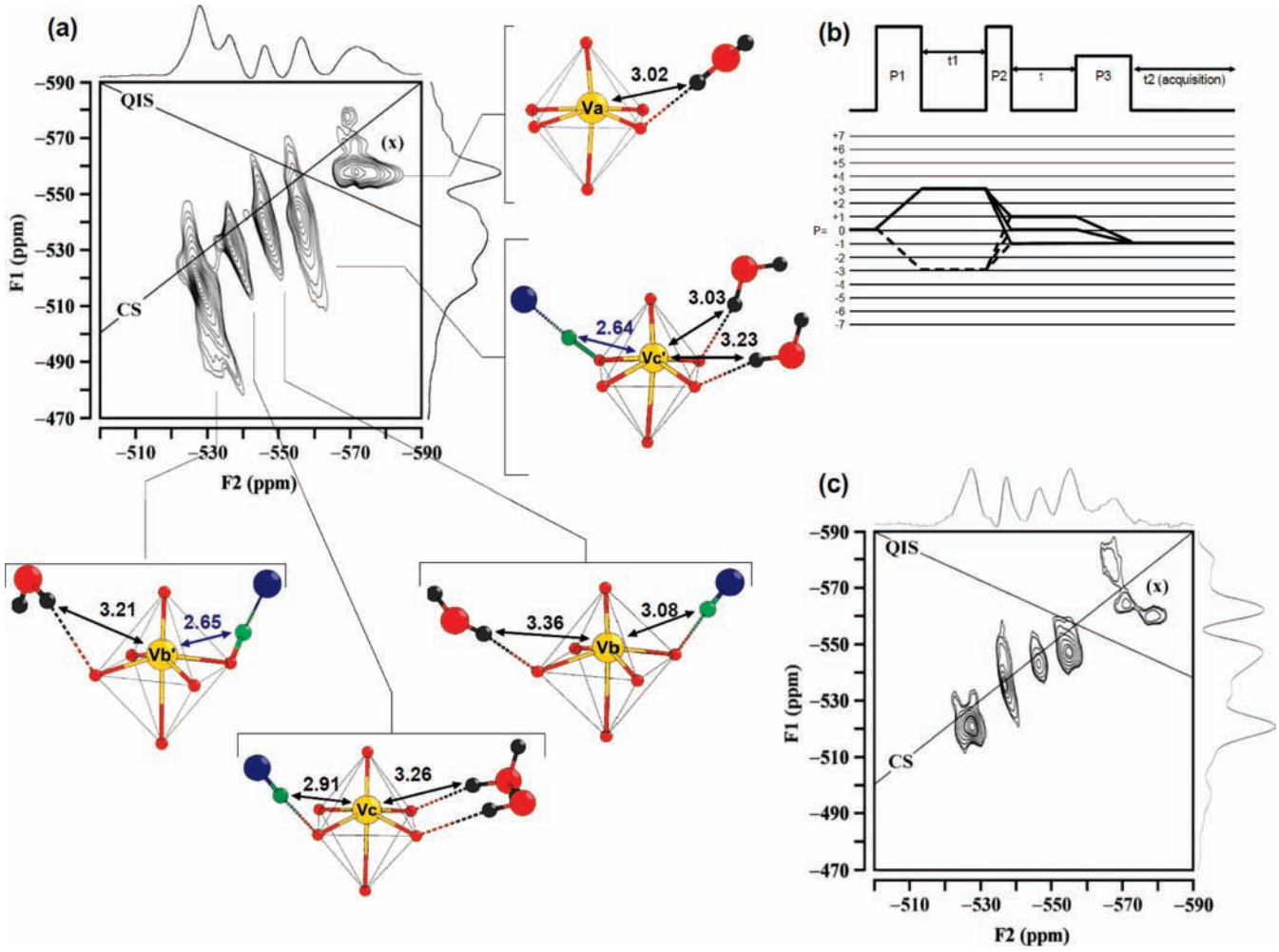

Figure 7. ^{51}V 3QMAS NMR spectra in the region around −500 ppm of $Cs_4[H_2V_{10}O_{28}]\cdot 4H_2O$ (a) without ^{1}H decoupling and (c) with ^{1}H decoupling. (x) corresponds to a spinning sideband. Assignment of the five resonances is depicted using polyhedral representations of the VO_6 sites, along with the nearest hydrogen atoms linked to water molecules (H atoms are green) and to the hydroxyl group (H and O atoms are in green and blue, respectively). Distances are given in Å. (b) Phase-modulated multiplex SPAM 3QMAS NMR pulse sequence.

The latter are characterized by short V···H distances around 2.6 Å, compared to the range of 2.9−3.4 Å for Vb and Vc. In the DVD structure, Vb′ and Vc′ are both donors and acceptors of hydrogen bonds, whereas Vb and Vc are only acceptors (Figure 7).

At this stage, we have to note that 3QMAS experiments could be useful for the estimation of small CSA parameters, as this interaction is also magnified by the MQ order in the isotropic dimension.[106,107] In the case of $Cs_4[H_2V_{10}O_{28}]\cdot 4H_2O$, accurate CSA parameters were already obtained from extensive fitting of ^{51}V 1D MAS spectra at various fields.[53]

6.3. Investigation of the Relationships between VO_6 Octahedral Deformations and ^{51}V NMR Parameters. Since the five optimized geometries present different distorted VO_6 sites, it is interesting to correlate these VO_6 geometries to ^{51}V NMR parameters. Relationships between ^{51}V NMR parameters and the local environment of vanadium were previously established on model compounds, including ortho-, pyro-, and metavanadates with well-known crystal structures.[46–49,51,52] However, this type of correlation was not properly defined for vanadates that exhibit VO_5 and/or VO_6 units. This is mainly due to the fact that only a small number of polyoxovanadates (mainly V_2O_5 and the $M[V_3O_8]$ compounds) with vanadium geometry differing from tetrahedral symmetry were previously characterized by ^{51}V MAS NMR spectroscopy.[108,109,53,54] Therefore, the decavanadate polyanion constitutes an interesting reference compound. By using the structural parameters defined in Figure 4a, it was possible to establish correlations with the ^{51}V NMR parameters C_q and $\Delta\delta$. Linear regressions plotted in Figure 8 give the relations:

$$d = -0.22C_q + 1.876 \; (R = -0.992) \qquad (15)$$

$$\alpha = -2.05C_q + 180.0 \; (R = -0.985) \qquad (16)$$

$$\beta = 1.47C_q + 88.5 \; (R = 0.949) \qquad (17)$$

$$\Delta\beta_m = -0.74C_q + 14.4 \; (R = -0.965) \qquad (18)$$

where C_q, d, and $\{\alpha, \beta, \Delta\beta_m\}$ are given in MHz, Å, and deg, respectively. The reliabilities ($0.95 < R < 0.99$) obtained by

(106) Nielsen, U. G.; Jakobsen, H. J.; Skibsted, J. *Solid State Nucl. Magn. Reson.* **2003**, *23*, 107–115.
(107) Nielsen, U. G.; Jakobsen, H. J.; Skibsted, J. *Solid State Nucl. Magn. Reson.* **2001**, *20*, 23–34.
(108) Fontenot, C. J.; Wiench, J. W.; Schrader, G. L.; Pruski, M. *J. Am. Chem. Soc.* **2002**, *124*, 8435–8444.
(109) Fontenot, C. J.; Wiench, J. W.; Pruski, M.; Schrader, G. L. *J. Phys. Chem. B* **2000**, *104*, 11622–11631.

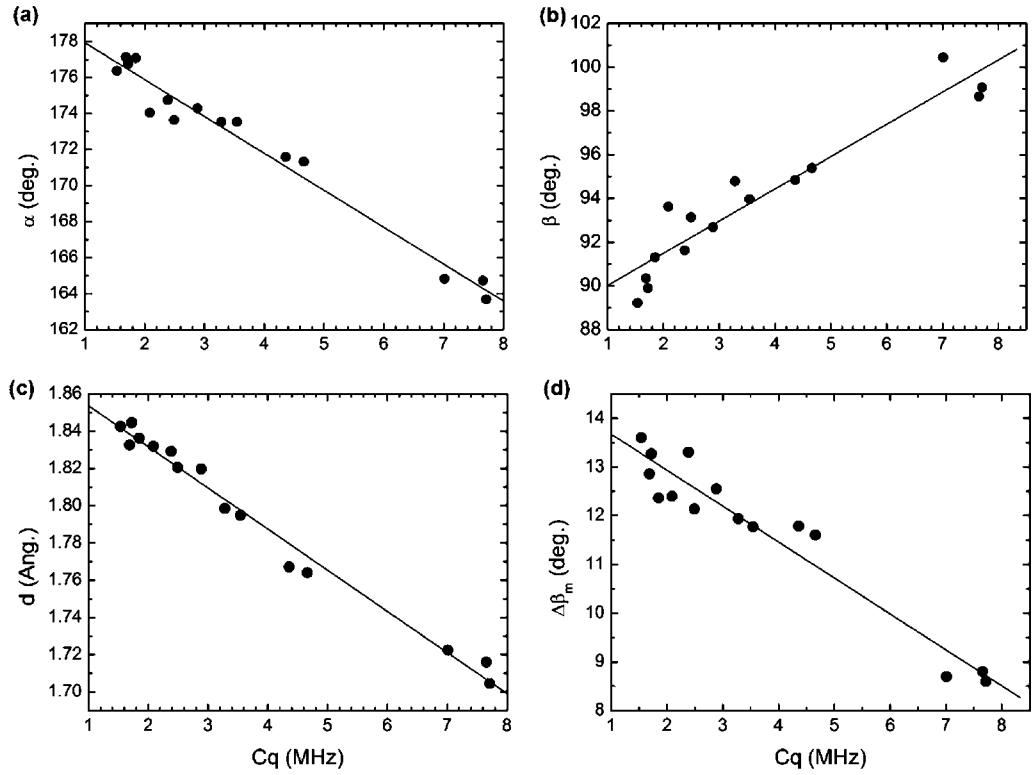

Figure 8. Theoretical ^{51}V quadrupolar constants from the O1-, O2-, and TS-DVD geometries plotted as a function of the structural parameters α, β and d defined in Figure 4a. The solid lines represent the linear correlations.

fitting the different distributions allow rather safe extractions of structural parameters such as V−O distances or O−V−O angles from the values of V quadrupolar constants. We note that, for the relations (16) and (17), the values of α and β at $C_q = 0$ are equal (or close) to 180 and 90°, respectively, which corresponds to the geometry of a perfect pseudo-octahedron (the octahedron could be deformed along one of the symmetry axes). Indeed, for a hypothetical VO_6 octahedron with a point symmetry O_h, the electric field equals zero. Finally, the correlation of C_q (in MHz) as a function of $\Delta\delta$ (in ppm) is defined by the relation

$$C_q = 0.047\Delta\delta + 20.6 \; (R = 0.952) \qquad (19)$$

This correlation is presented in Figure S2 of the Supporting Information. This reveals that the shielding anisotropy and quadrupolar constant give the same information about the VO_6 polyhedron deformation within the decavanadate polyanion.

7. Conclusions

This work has demonstrated that the combination of first-principles calculations and ^{51}V solid-state NMR experiments can be combined in order to refine with accuracy the complex structure of an inorganic system containing five nonequivalent distorted VO_6 sites within a decavanadate polyanion. From the study case of $Cs_4[H_2V_{10}O_{28}]\cdot 4H_2O$, we have observed that, whereas the comparison of calculated and experimental ^{1}H NMR parameters does not allow us to distinguish between the possible isomers, the high sensitivity of ^{51}V NMR parameters with respect to the hydrogen-bond network can be sufficiently reliable to definitively resolve the location of the surface hydroxyl ligands. The predicted NMR parameters, and particularly the quadrupolar parameters, are fully consistent with the experimental data, allowing the first assignment of the five ^{51}V resonances for a decavanadate reported to date. In order to confirm these results, ^{51}V 3QMAS NMR spectra of $Cs_4[H_2V_{10}O_{28}]\cdot 4H_2O$ were recorded. By taking into account that ^{1}H−^{51}V dipolar coupling is enhanced during the triple quantum evolution, the comparison of ^{51}V 3QMAS NMR spectra recorded with and without ^{1}H decoupling has allowed us to identify the vanadium sites coordinated by an OH ligand, in full agreement with first-principles calculations. Moreover, relationships have been established between NMR parameters (C_Q and $\Delta\delta$) and structural parameters (V−O distance, O−V−O angle). Such correlations will be particularly useful to characterize a wide range of polyoxovanadates and vanadium oxides with VO_6 units.

Finally, on a more general level, this study confirms that combining X-ray diffraction and experimental and computational multinuclear NMR can be a powerful and elegant way to resolve a wide range of crystallographic structures. Since solid-state NMR is a nonperturbing method and chemical shift and quadrupolar coupling constants are known to be excellent probes for molecular conformation and intermolecular interactions, such a methodology may have numerous perspectives in the fields of solid-state or inorganic chemistry, biochemistry, and organic chemistry. We stress also the fact that the GIPAW/NMR approach, including explicitly the systematic evaluation of the theoretical errors and a statistical modeling of the experimental data, should be generalized to a large number of hybrid organic/inorganic systems.

Acknowledgment. We thank Dr. F. Fayon (CEMHTI, UPR3079 CNRS, France) for fruitful discussions about the

interpretation of ^{51}V 3QMAS NMR spectra and M. Paris for the ^{1}H NMR experiments. Computations presented in this work were performed at the CCIPL "Centre Régional de Calcul Intensif des Pays de la Loire" financed by the French Research Ministry, the "Région Pays de la Loire", and the University of Nantes. The CCIPL is also thanked for the financial support related to the CASTEP license. L.A.T. gratefully acknowledges D. Hache for graphic arts and M. Rudolph for careful reading of this paper. Finally, we thank the three anonymous reviewers for very helpful comments and suggestions.

Supporting Information Available: Tables, figures, and CIF files giving theoretical and experimental ^{51}V NMR parameters for the whole set of vanadium oxide compounds and $Cs_4[H_2V_{10}O_{28}]\cdot 4H_2O$, selected structural parameters for $Cs_4[H_2V_{10}O_{28}]\cdot 4H_2O$, additional experimental ^{51}V MQMAS and simulated ^{1}H spectra, and the $\Delta\delta/C_q$ correlation not shown in the main paper. This material is available free of charge via the Internet at http://pubs.acs.org.

JA908973Y